

# PARTICLE WORLD

Technical Papers  
of 3P Instruments  
EDITION 25  
SEPTEMBER 2024

**Bettersize S3 Plus** for optimizing battery electrode properties

Investigation of the **separation properties** of membranes

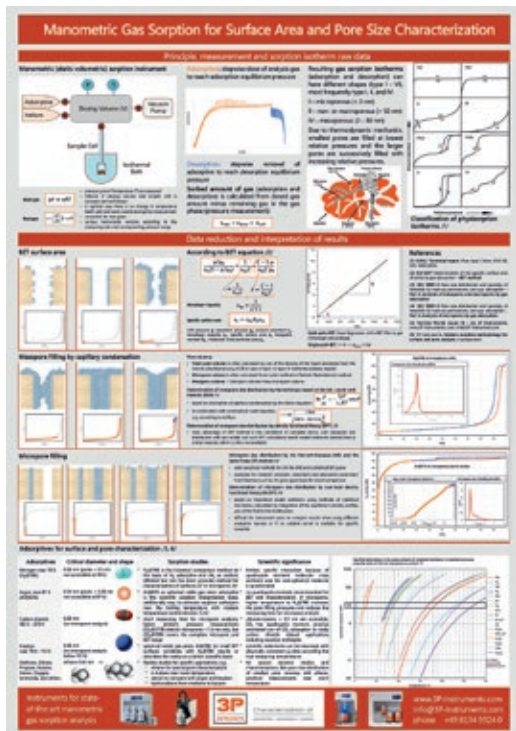
**isoTune** - the next generation in sorption science

**BeScan Lab** for accurate dispersion stability analysis



# Contents

- **Bettersizer S3 Plus:**  
Influence of particle morphology of the active material properties on lithium-ion battery electrode properties.....3
- **BeNano series light scattering in life sciences -**  
Now with DLS microrheology and DLS flow mode option for enhanced protein analysis ..... 8
- **BeScan Lab - The new benchmark in stability analysis.....**13
- **News .....15**
- **Studies on the optimal characterization**  
of smallest portions of porous structures .....17
- **Development of a comprehensive measurement system**  
for membrane separation properties.....21
- **The isoTune - The next generation**  
in sorption science.....27



## Imprint

**Publisher:**  
3P Instruments GmbH & Co. KG  
Rudolf-Diesel-Straße 12  
85235 Odelzhausen | Germany  
Tel. +49 8134 9324 0  
info@3p-instruments.com  
www.3p-instruments.com

**Editor-in-Chief:**  
Dr. Dietmar Klank

**Illustrations:**  
3P Instruments, Adobe Stock

**ISSN 2750-7084 (Print)**  
**ISSN 2750-7092 (Online)**

Dear Readers,



the Particle World is back and this no. 25 edition reports once again news, experiences, results and developments in the field of characterization of powders, particles and pores. The increasingly well-known international 3P Instruments has recently been particularly successful with

- mixSorb analyzers to study mixed gas and vapor sorption delivered to companies and institutes e.g. in Brazil, Canada, China, France, Qatar, Saudi Arabia and USA
- further developments as the European distributor together with our international partners for the high-tech Bettersize instruments, with new customers in Belgium, France, Germany, Portugal, Spain, Sweden, Switzerland and UK
- electro-acoustic instruments from Dispersion Technology to characterize high-concentrated slurries, e.g. in battery application
- many events and activities, e.g. the annual meeting on adsorption & characterization of porous solids 2024, a series of webinars, participation on Powtech, Analytica, Achema and other exhibitions, a huge amount of test and contract measurements in our Lab for Scientific Particle Analysis, and others.

The Bettersizer S3 Plus, with its unique combination of parallel laser diffraction and image analysis with two CCD camera units is increasingly becoming the benchmark for the investigation of particle size distributions with parallel particle shape estimation. On p. 3 we present a Bettersizer S3 Plus study of the influence of particle morphology of the active material properties on lithium-ion battery electrode properties.

Another enormously important field is the characterization of proteins in life sciences, where the Bettersize BeNano series combines the Dynamic Light Scattering with DLS microrheology and DLS flow mode option for enhanced protein analysis, see at p. 8.

3P Instruments has started a new research project recently, co-financed by the European Union and the Federal State of Saxony, to develop a novel analytical device for the optimal characterization of the smallest pore volumes and the associated pore size distributions. If you have to study materials with very low contents of pores below 500 nm, feel free to contact us for a test of the new sorption method currently under development (see outlook at p. 17).

We would like to point out other great developments in the field of sorption, one about a new measuring system for membrane separation properties, see at p. 21. And you will find a real highlight on p. 27 with the unique isoTune sorption analyzer as the pioneer of the next instrument generation in sorption science. Be sure, the isoTune will make an impression the sorption community with special sorption studies in the next Particle World!

Last but not least, feel free to take note of the tiny poster on this page "Manometric Gas Sorption for Surface Area and Pore Size Characterisation" for all sorption instrument users. We will be happy to send you the print data or a direct printout for your lab. Enjoy reading and all the best for you!

Dr. Dietmar Klank and the 3P Instruments team

# Bettersizer S3 Plus: Influence of particle morphology of the active material properties on lithium-ion battery electrode properties

Dr. Christian Oetzel, christian.oetzel@3P-instruments.com



## Introduction

As the energy transition takes place in industrialized countries, batteries are playing an increasingly important role as energy storage devices. Due to their long service life and energy density, modern lithium-ion batteries are currently a particular focus of research and development.

The electrode production of this type of battery is usually carried out using a wet coating process on the carrier foil via the suspension route. For the anode, the starting materials of the suspension are often mixtures of graphite, carbon black and water as well as binders and additives for optimal adjustment of the viscosity and particle dispersion. The cathode slurry consists mainly of lithium-nickel-manganese-cobalt oxide (NMC), usually dispersed in N-methyl-2-pyrrolidone (NMP) as a dispersion medium [1]. Interesting alternative materials are, for example, LCO (Lithium Cobalt Oxide) or LFP (Lithium Iron Phosphate).

In the following article the extent to which morphological properties of the starting powders influence key battery properties is discussed. In addition, the Bettersizer S3 Plus is presented as a suitable measuring device for determining relevant morphological parameters.

## Important battery properties and the influence of particle morphology

Key battery characteristics are essentially energy density, power density, life span, safety and manufacturing plus follow-up costs. This article looks at the first three in particular.

The morphological properties of a powder can be described first by the relative particle size distribution and second by specific particle shape parameters. If the shape of a particle corresponds to that of an ideal sphere and the individual particles are also

of almost the same size, the parameter "mean particle size" is basically sufficient to describe the morphology. However, this is usually not the case with the real materials used for battery electrodes. Typical graphite or NMC powders always have a certain size distribution and shape anisotropy (see Figure 1).

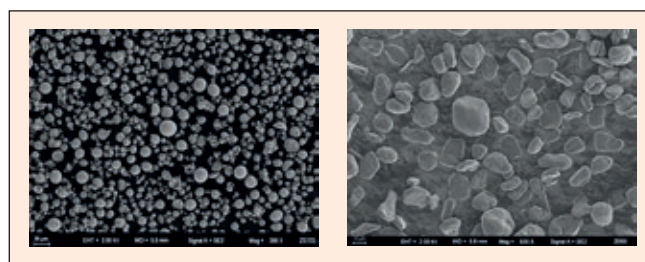


Figure 1 SEM-pictures of a NMC powder (left) and graphite powder (right) used for battery electrodes

For these powders, it therefore makes sense to specify one or more suitable shape parameters in addition to an equivalent diameter distribution function in order to describe the morphology. Interesting shape parameters for the packing behavior of the particles are circularity and aspect ratio. Details of these and other interesting parameters can be found in [2].

For the size ranges of the relevant materials for battery slurries, laser diffraction is a suitable method. The measured particle size is therefore a scattered light equivalent diameter or its volume distribution function [3].

In the following chapter, the main battery properties are discussed in detail with regard to the influence of particle morphology.

**Figure 2**  
Influence of the morphology of the electrode layer of a battery on energy density and power density

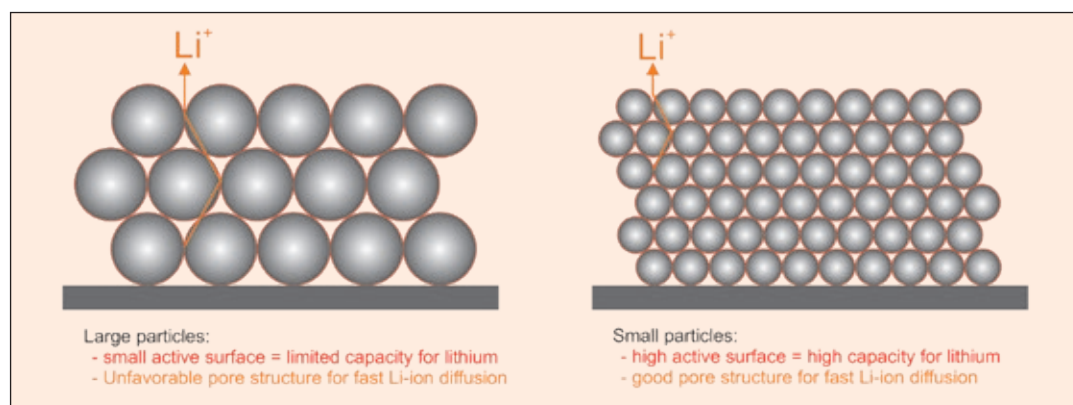
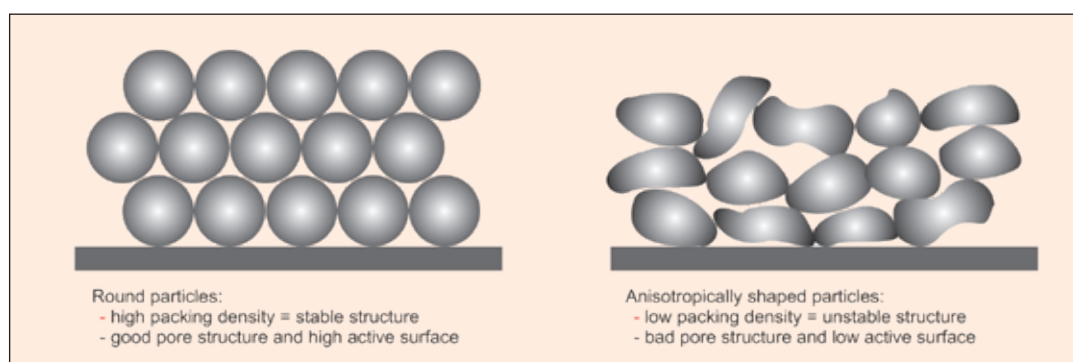


**Figure 3**  
Influence of particle shape inhomogeneities of the active material on the electrode layer of a battery



## Energy density

A high energy density means that a large amount of carrier material (Li) can be stored in a relatively small electrode (or battery) volume and correspondingly more energy can be provided over a longer period of time (during a discharging process). This battery property is significantly influenced by the available active surface of the electrodes and their accessibility (pore structure, see Figure 2).

This property (active surface) and also the packing behavior and thus the pore structure of the battery electrode are significantly influenced by the particle size distribution and shape of the particles of the active starting material. The fact is that the particles must not be too large or too small, but that the particle size and distribution width must be optimal in the medium size range in order to achieve the best possible energy density. Furthermore the packing structure of the layer is determined by the modality and the ratio of the particle sizes of the modes. For example, in order to obtain higher-packed structures, the particles of a second mode must be correspondingly small in order to fill the spaces between the larger particles well within the electrode layer.

In addition, it is advantageous for the geometry of the particles to be as spherical as possible (see Figure 3), as the packing density and homogeneity decreases with increasing shape anisotropy. Only if the pore channels are homogeneous and well permeable the "occupancy sites" in the rear areas of the layer can be easily reached by the charge carriers. For the aspect ratio and circularity as parameters, this means that values close to 1 are desirable in both cases.

## Power density

In case of a high power density the charge carrier exchange during charging and discharging of the battery takes place quickly and therefore a high voltage is possible during operation and rapid recharging afterwards. As with the energy density, an ideal pore structure is required here (see Figure 2 and 3). Similar to the energy density, an ideal pore structure and high active surface area are required to ensure fast and continuous charge carrier transport.

As with the energy density, the particle size distribution and shape (e.g. circularity, aspect ratio) are therefore important properties of the starting powders that influence the battery power density.

## Life span

The ageing processes in a lithium-ion battery have not yet been fully clarified [4]. However, the chemical processes at the electrolyte/active material interface during charging and discharging certainly play an important role here. In addition to the formation of passivation layers, this can lead to cracking or chipping of the active material surface, for example.

A key influencing parameter is therefore again the shape and size of the active material powder. In principle smaller and less round particles tend to break more during the charging and discharging cycle. On the other hand, larger particles mean poorer energy and power density.

In order to optimize all three of these battery properties simultaneously, the size and distribution of the output powder particles must also be within certain ideal ranges. In addition, the roundest possible shape is advantageous for all properties.



**Figure 4** *Bettersizer S3 Plus:*  
Combination of laser diffraction and dynamic image analysis;  
left: instrument picture;  
right: instrument setup incl. DLOI-technology and  
CCD camera unit (X0.5 and X10)



Irregular agglomerate structures that form in the battery paste during the process are also a disadvantage for the service life. The aim here is to prevent this effect as far as possible by means of a large zeta potential of the powder particles in the liquid [5].

A comprehensive particle morphology analysis can be carried out with the Bettersizer S3 Plus [6]. In the following chapter, this measuring device is first briefly introduced and then its capabilities are demonstrated using the example of various powders used to manufacture battery electrodes.

## Experimental setup and results

### Measurement device and analysis conditions

The Bettersizer S3 Plus (Figure 4) is an analytical instrument that combines laser and image techniques for a comprehensive characterization of particle size and morphology. It allows the analysis of particle size distribution from the nano to the millimeter range by means of classical laser diffraction. Additionally, the simultaneous characterization of particle shape as well as oversized grains and agglomeration phenomena by means of dynamic image analysis (micrometer to millimeter range) is possible.

In addition to an innovative design of the optical bench (DLOI-technology = Dual Lenses & Oblique Incidence, Figure 4 right) with a short-wave green laser and a wide scattering angle coverage of  $0.02 - 165^\circ$ , two benefits of the instrument in particular should be pointed out:

- Real time particle size and shape determination using a synchronously working double CCD camera system (size: 2 - 3500  $\mu\text{m}$ , shape:  $\geq 4 \mu\text{m}$ )
- Combination of laser diffraction and image analysis for a precise particle size distribution, especially in the coarse grain edge area, also for oversized particle analysis

A good overview of the most important details about the measuring device can be found in [7].

To demonstrate the capabilities of the Bettersizer S3 Plus for the morphology study of battery electrode materials, samples were taken from an NMC-111-NMP slurry and an aqueous graphite suspension, which are used for electrode coating (NM C-111: lithium-nickel-manganese-cobalt oxide powder with a nickel:manganese:cobalt ratio of 1:1:1). The samples were directly analyzed in terms of particle morphology via dilution in the respective dispersion medium in a Bettersizer S3 Plus. The tests in water were performed with the standard dispersion unit (BT-803), the experiments in NMP with the small volume solvent resistant unit (BT-80N Pro). After adding the samples to the dispersion unit, both were sonicated for 120 s with 35 W and the particle size distribution was measured using laser diffraction. Immediately afterwards, the particles were photographed and analyzed in real time using the high-resolution dual CCD camera system (dynamic image analysis, X0.5 camera for particles in the range of 30 – 3500  $\mu\text{m}$ , X10 for particles between 2 and 100  $\mu\text{m}$ ).

### Particle size distribution and oversize particle analysis

Figure 5 shows an overlay of the measured particle size distribution of graphite and NMC-111, measured by laser diffraction. Both samples were stable to measure, further ultrasonic treatment had no influence on the respective size distributions.

Images of the individual particles of both samples, graphite and NMC-111, with the maximum size of both distributions are shown in Figure 6.

In the case of graphite, oversized grains or agglomerates, which cannot be detected in the particle size distribution measured with laser diffraction alone (Figure 5) due to statistical inaccuracy in the coarse range, were detected using the X0.5 CCD camera. However, such structures can lead to inhomogeneities in the active material layer during the manufacture of the electrodes. It is therefore desirable to minimize such superstructures. Consequently, their identification by dynamic image analysis is crucial during the production process.

In the case of NMC-111, such oversized particles could not be found with either the X0.5 or X10 camera, all photographed particles were within the measured size distribution shown in Figure 2.

A short summary of the particle size analysis of both powders is given in table 1.

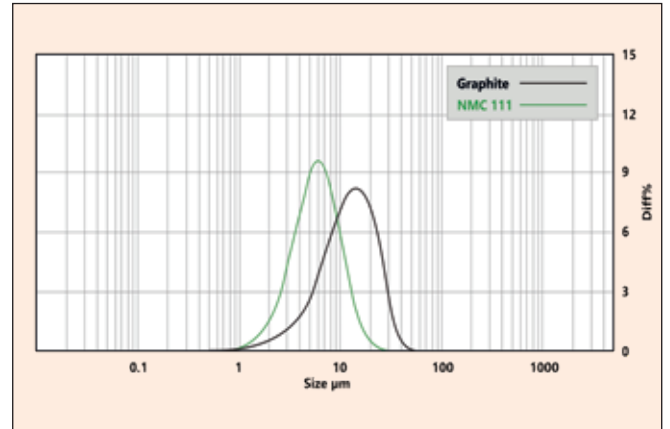


Figure 5 Particle size distribution of graphite and NMC-111, measured using the Bettersizer S3 Plus by means of laser diffraction

### Particle shape analysis

For the present battery starting powders, the shape analysis of the powders is focused on the parameters circularity and aspect ratio.

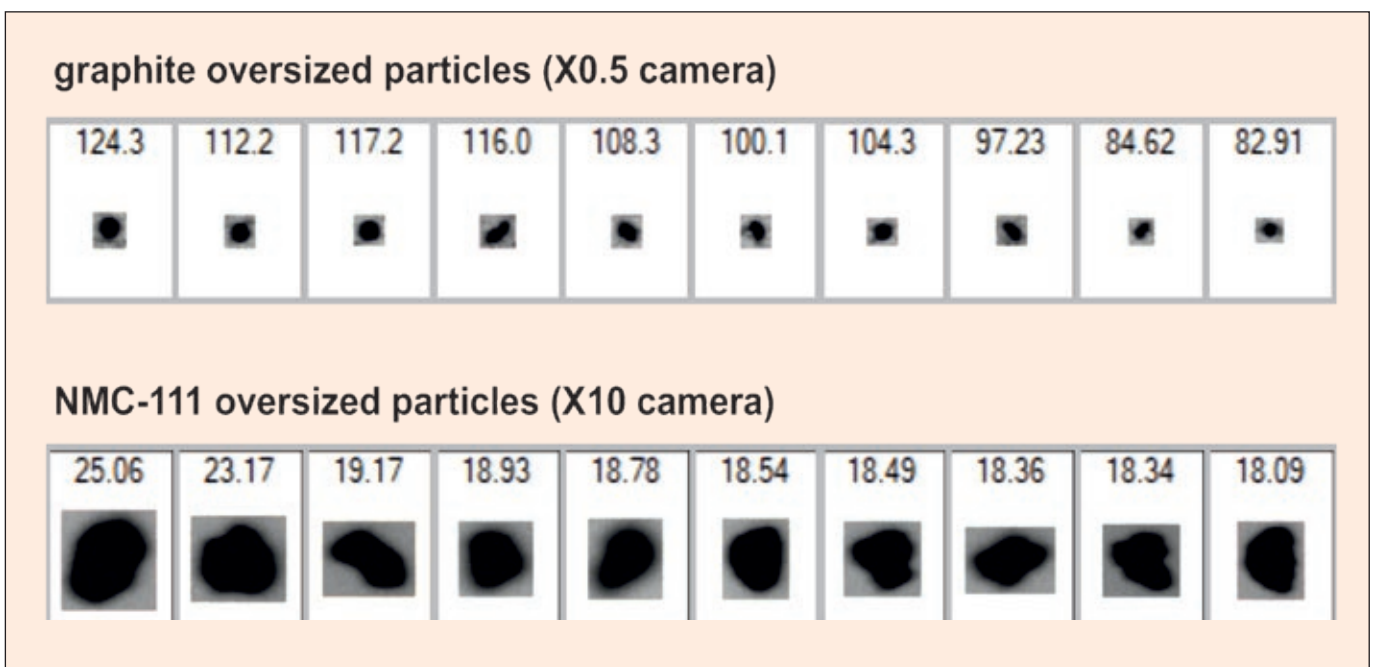


Figure 6 Oversized grains of graphite and NMC-111, the specified diameter represents the area equivalent diameter [μm] [3]

Table 1 Particle size analysis results of graphite and NMC

Sample	D10 [μm]	D16 [μm]	D50 [μm]	D75 [μm]	D84 [μm]	D90 [μm]	Oversized particles
Graphite	4.908	6.193	7.875	18.32	21.52	24.58	not present
NMC-111	2.610	3.161	3.881	5.697	9.483	10.93	present: max. detected particle 124.3 μm

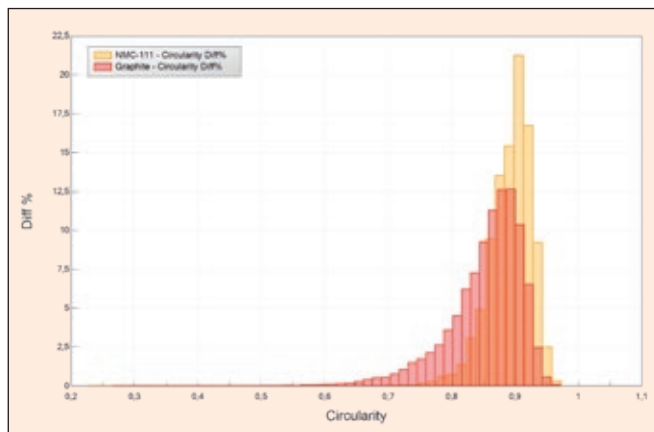


Figure 7 Number distribution of circularity of graphite and NMC-111

Figure 7 shows the number distribution curves of the circularity of graphite and NMC-111. About 40,000 particles were taken into account for the evaluation in each case; only particles larger than 5  $\mu\text{m}$  were considered.

Obviously, graphite shows a much wider distribution of circularity, which, according to the above analysis, could be improved for the properties of the battery, as the overall grain shape should be as spherical as possible. Figure 8 shows the dependence of the circularity of both samples on the particle size in a point cloud diagram.

NMC shows significantly better roundness than graphite over the entire size range. In Figure 9 the aspect ratio of both materials vs. equivalent area diameter instead of the circularity is presented.

The NMC-111 particles on average have a significantly lower elongation than the graphite particles and therefore show a more favorable packing structure in the electrode layer in comparison to graphite at otherwise identical conditions.

Table 2 summarizes the results of the shape analysis on graphite and NMC. It should be noted at this point that, in addition to the initial powder morphology, the dispersion state of the particles in the battery slurry and further properties like viscosity or electric conductivity have a major influence on the final electrode properties [5]

## Conclusion

The article discussed the influence of particle size distribution and shape on the main battery properties. In order to achieve an optimum pore structure and packing density in the electrode layer, the particle size and particle distribution must reach a certain optimum. The particle shape should be as spherical as possible.

Table 2 Particle shape analysis results of graphite and NMC

Sample Name	Circularity Distribution					Aspect ratio distribution				
	C5	C10	C50	C90	C95	A5	A10	A50	A90	A95
Graphite	0.738	0.775	0.866	0.914	0.923	0.391	0.439	0.629	0.808	0.846
NMC-111	0.832	0.849	0.899	0.932	0.939	0.545	0.581	0.725	0.847	0.872



Figure 8 Circularity vs. equivalent area diameter of graphite and NMC-111

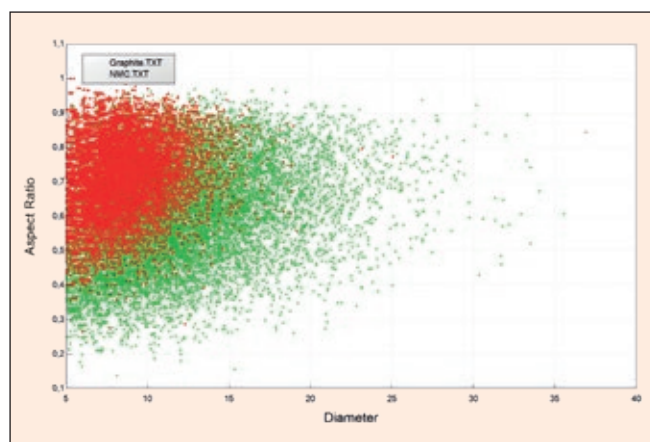


Figure 9 Aspect ratio vs. equivalent area diameter of graphite and NMC-111

Furthermore, it was shown that the Bettersizer S3 Plus is capable of performing a comprehensive particle size and shape analysis for particles used in the battery sector. This was demonstrated with two powders used in the battery sector, NMC and graphite.

## References

- [1] „Produktion einer All-Solid-State-Batteriezelle“ in <https://www.pem.rwth-aachen.de/go/id/rtzd>
- [2] ISO 9276-6:2008-09, Representation of results of particle size analysis – Part 6: Descriptive and quantitative representation of particle shape and morphology, Beuth, Berlin 2008.
- [3] ISO 13320:2020-01, Particle size analysis - Laser diffraction methods, 2020.
- [4] S. R. Käbitz; „Untersuchung der Alterung von Lithium-Ionen-Batterien mittels Elektroanalytik und elektrochemischer Impedanzspektroskopie“, Dissertation, 2016, RWTH Aachen; <https://publications.rwth-aachen.de/record/680923/files/680923.pdf>
- [5] C. Oetzel; „Akustische Methoden in der Batterieforschung; Appnote 6-01; 3P Instruments; 03.2024; <https://www.3p-instruments.com/wp-content/uploads/2024/05/3P-APPNOTE-6-01-App-Note-3P-Akustische-Methoden-in-der-Batterieforschung.pdf>
- [6] [https://www.3p-instruments.com/analyzers/bettersizer\\_s3\\_series/](https://www.3p-instruments.com/analyzers/bettersizer_s3_series/)
- [7] [https://www.3p-instruments.com/wp-content/uploads/2017/03/PARTICLE-WORLD-6\\_low.pdf](https://www.3p-instruments.com/wp-content/uploads/2017/03/PARTICLE-WORLD-6_low.pdf)

# BeNano series light scattering in life sciences - Now with DLS microrheology and DLS flow mode option for enhanced protein analysis

Dr. Marion Ferner, marion.ferner@3P-instruments.com



## Introduction

Proteins are the building blocks of life and play a decisive role in biological processes. The following examples illustrate their importance and diversity:

- enzymes (control of metabolism)
- hormones (e.g. insulin - regulation of blood sugar level)
- antibodies for immune system response
- structural proteins for cells and tissue (e.g. muscle fibres, organs)
- transport proteins (e.g. haemoglobin - transport of oxygen)
- storage proteins (e.g. ferritin - storage of iron)
- receptors for biomolecules in signalling (e.g. in nerve cells)

This diversity requires coordinated biosynthesis. The basic building blocks of proteins are amino acids, organic compounds that are strung together like pearls (specific to each protein). The amino acid sequence (primary structure) of a protein is genetically determined in the DNA sequence of an organism. However, proteins only achieve structural stability through interactions between non-adjacent amino acids and thus through folding into higher-level, three-dimensional structures (tertiary structure). In addition to intramolecular interactions (monomer -

interaction of amino acids of one protein molecule), intermolecular interactions (dimer, trimer, multimer - interaction of amino acids of two, three or more protein molecules) lead to the formation of complex quaternary structures. These three-dimensional structures are specific to each protein of an organism and are essential for its functionality. Even small errors can lead to a complete loss of function.

The complexity of proteins makes them interesting objects for research and development, both in basic research and in the development and production of biotherapeutics. **Particle size, zeta potential/charge, molecular mass, microrheological properties and stability are essential protein parameters** during enrichment, engineering (recombinant proteins), process development (e. g. of biopharmaceuticals) and quality control. Optimised conditions are an important prerequisite to guarantee proteins' in vitro integrity, functionality and stability. Stress factors like temperature, buffer pH, salt content or ageing during storage can lead to alteration of biophysical characteristics due to protein denaturation (e.g. destruction of tertiary and/or quaternary structure) or aggregation (Fig. 1).

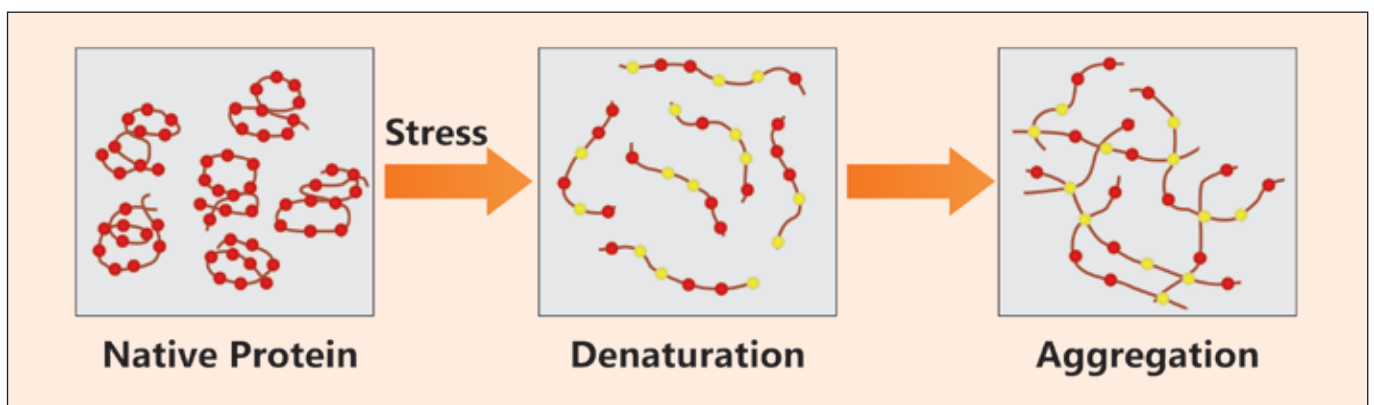


Figure 1 Protein denaturation and aggregation



Instruments of the BETTERSIZE BeNano series particle analysers are a helpful tool in biomolecules' analysis. The implemented light scattering methods provide insights into structural changes of macromolecules like proteins. Dynamic light scattering (DLS), electrophoretic light scattering (ELS) and static light scattering (SLS) can be used for particle size, zeta potential and molecular mass determination [1]. In addition, equipped with the fully automated titrator BAT-1, the determination of the isoelectric point is also possible [2]. Besides these general parameters, viscoelastic properties (e. g. complex viscosity), determined by the new BeNano DLS microrheology (DLS $\mu$ R) option as well as the DLS flow mode option for high-resolution size distribution measurements, can also be important in structural and functional analysis of proteins.

### Dynamic light scattering microrheology (DLS $\mu$ R) in protein analysis

DLS $\mu$ R is a technique that uses the Brownian motion of tracer particles of known size in dynamic light scattering to investigate the viscoelastic properties of complex systems such as weakly structured protein from the measured mean square displacement (MSD,  $\Delta r^2$ ) (see [2] for details). The MSD is a measure of the volume that the tracer particles migrate on average in a certain time period, which means that the faster the particles diffuse, the greater the MSD and in consequence the lower the complex viscosity of the analysed system.

The principle of DLS $\mu$ R is shown in Fig. 2. The rheological properties of the environment are reflected in the motion of the tracer particles. For a purely viscous fluid sample (Newtonian fluid) like water, the tracer particles diffuse freely throughout the sample and the MSD of the particle increases linearly with time. In contrast, for a non-Newtonian fluid like a protein solution

which contains elastic components, the tracer particles are hindered in free diffusion.

The MSD vs. time curve is directly related to the frequency-dependent generalized Stokes-Einstein equation, which in turn contains the elastic and viscous components  $G'$  and  $G''$  of the system (equation 1).

$$G^*(\omega) = \frac{k_B T}{\pi R i \langle \Delta r^2(i\omega) \rangle} = G'(\omega) + iG''(\omega) \quad (1)$$

- $k_B T$ : thermal energy
- $R$ : radius of tracer particle
- $G'(\omega)$ : elastic (storage) modulus
- $G''(\omega)$ : viscous (loss) modulus
- $G^*(\omega)$ : complex modulus

The complex viscosity  $\eta^*(\omega)$  can then be obtained, respectively

$$\eta^*(\omega) = \frac{G^*(\omega)}{\omega} \quad (2)$$

### Example: DLS $\mu$ R in denaturation analysis of Bovine Serum Albumin

Bovine Serum Albumin (BSA) protein is widely used in protein research. As mentioned above, proteins are sensitive to stress conditions, e.g. buffer composition or heat stress. The mean particle size of BSA in water is around 3 nm, which is below the literature value of the BSA monomer (~7 nm) and may indicate denaturation of BSA in water [1]. When incubating BSA at different temperatures, it can be seen from particle size analysis using DLS, that it is relatively stable at moderate temperatures [1].

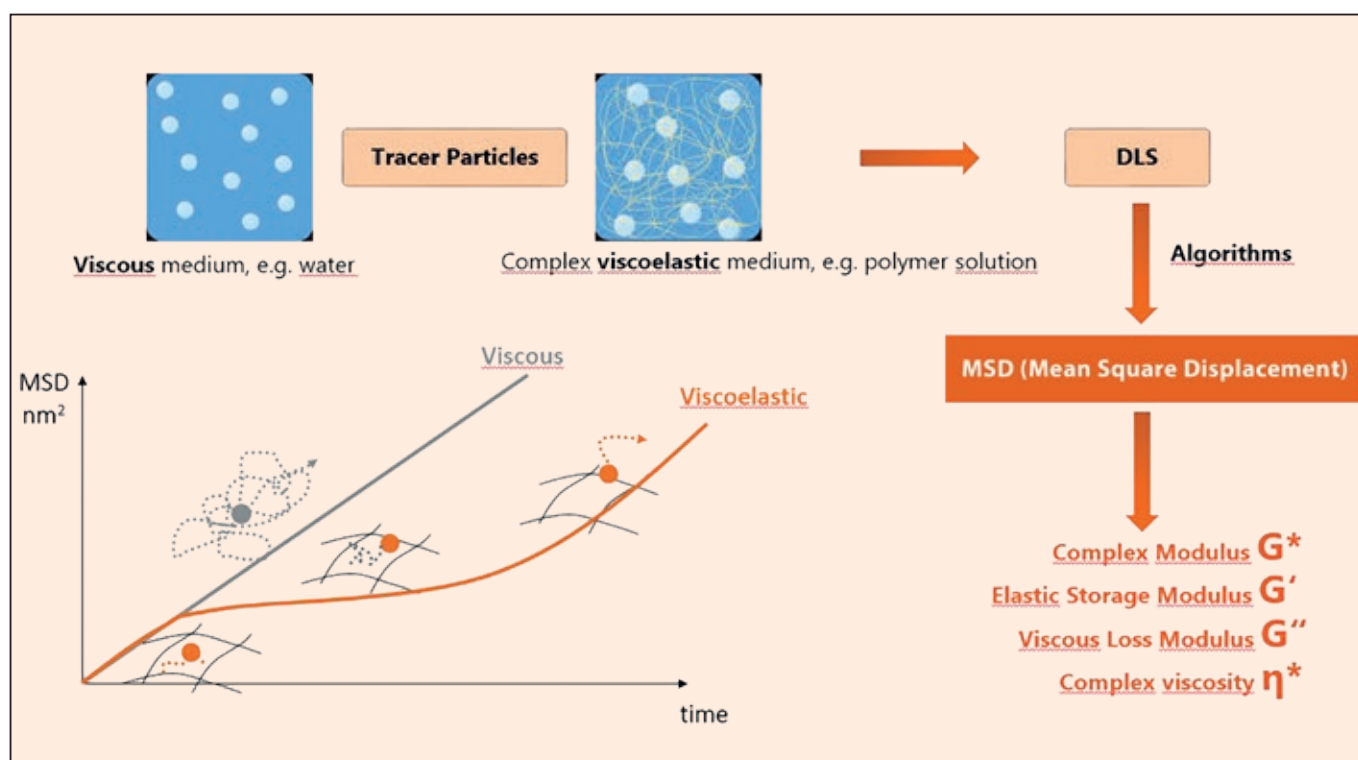


Figure 2 Principle of DLS $\mu$ R

With rising temperature, particle size increases above 65°C and up due to unfolding and aggregation as a consequence of denaturation. This leads to alterations of the protein solution. Emphasizing on the protein solutions properties, DLSµR helps to detect the denaturation and aggregation process, which is not obvious from the BSA particle analysis alone.

In the following experiment BSA (5 % in water) was incubated at temperatures of 25°C, 50°C, 70°C and 80°C and analysed for differences in viscoelastic properties during denaturation and aggregation using DLSµR of the BeNano 180 Zeta Pro. Polystyrene particles of 340 nm in size were used as tracer. By calculating the fluctuation of the scattered signals, the correlation functions and in consequence the MSD curves are obtained.

Fig. 3 shows the MSD curves of BSA at different temperatures in comparison. The MSD increases as the temperature rises from 25°C to 70°C indicating that the velocity of the tracer particles increases for this temperature range at decreasing solution viscosity (Fig. 4). It can be assumed that this viscosity decrease may be caused by conformational changes of BSA without being obvious from BSA particle size differences between 25°C and 50°C (Table 1). However, with increasing temperature above 70°C, the velocity of the tracer particles and in consequence the MSD decreases significantly. The formation of aggregates by the thermal denaturation of BSA results in increased solution viscosity.

Table 1 shows the temperature dependent values of the complex viscosity of the system at a frequency of 2096 rad/s

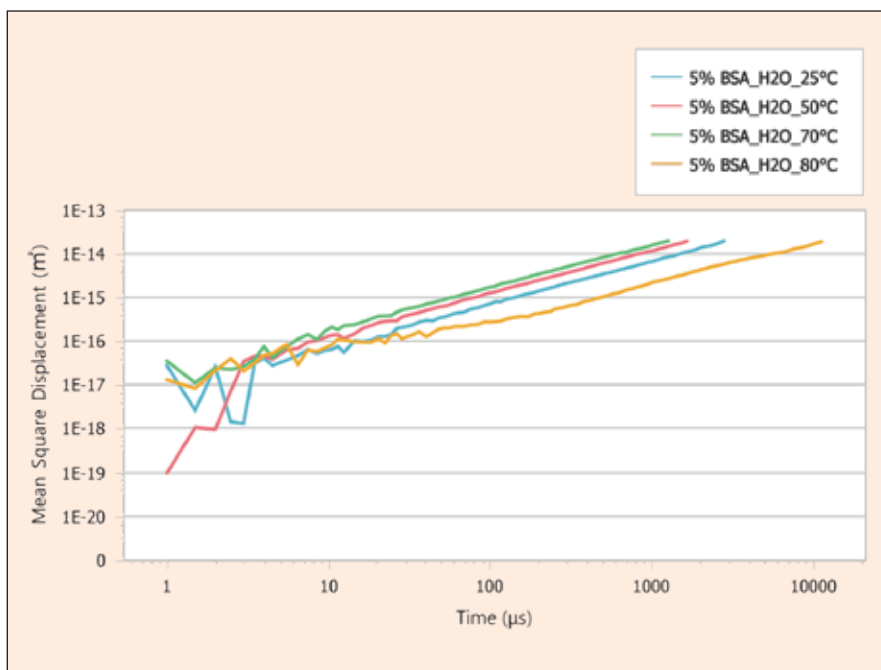


Figure 3 MSD curves of BSA solutions (5% in water) at different temperatures – BeNano 180 Zeta Pro

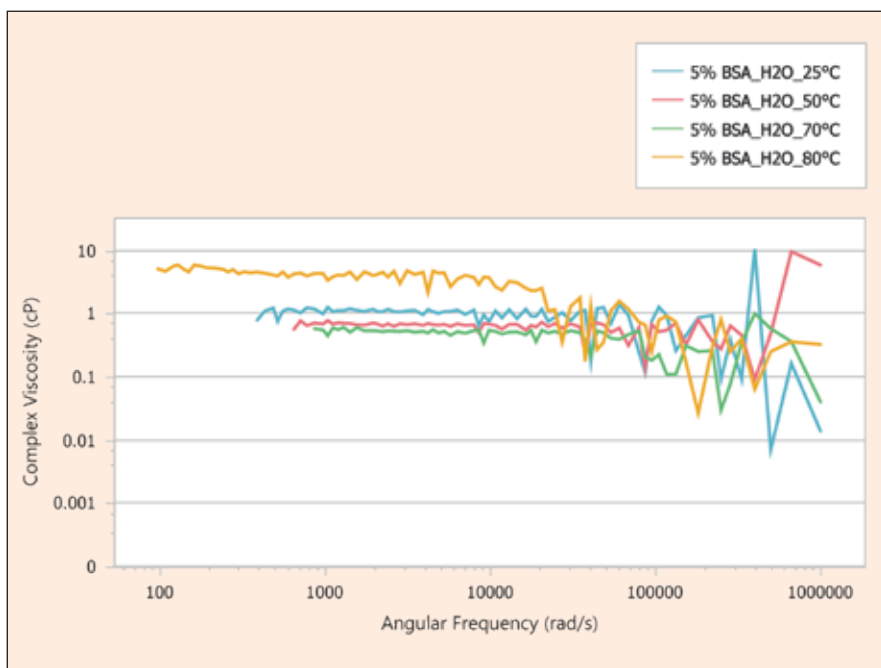


Figure 4 Complex viscosity of BSA solutions (5% in water) at different temperatures – BeNano 180 Zeta Pro

Table 1 Heat denaturation of BSA (5 % in water): Particle size and complex viscosity – BeNano 180 Zeta Pro

Temperature [°C]	Particle size Z-ave [nm]	Complex viscosity @2096 rad/s [mPa.s]
25	2.91	1.01
50	2.83	0.68
70	20.27	0.53
80	19.33	4.23

in comparison to BSA particle size during heat denaturation. The complex viscosity obtained by DLS<sub>μ</sub>R serves to cross verify protein alteration during denaturation and aggregation. At high temperatures protein denaturation leads to gelation and therefore increasing complex viscosity of the BSA sample. Particle size analysis using DLS is therefore limited and size results can be misinterpreted.

### DLS flow mode in protein analysis

Classical DLS is a widely used batch-mode technique for size distribution determination of finely distributed, small particles in suspension or polymers in solution. In general, due to limited size resolution, individual components in broad distributed samples can only be separated with a 2.5-3 times difference in particle size. This greatly limits the quantitative nature of size distribution results.

The DLS flow mode of BETTERSIZE BeNano series particle size analysers is a high resolution DLS technique in combination with front end sample separation equipment (Fig. 5). Monodisperse fractions, which are separated from a batch sample e.g. by gel permeation chromatography (SEC) or field flow fractionation, flow through the BeNano in a sequence of size to be analysed

by DLS. Each effluent component is ideally mono-dispersed or closely mono-dispersed with a resolution as high as 1.3:1. Size measurements of separated fractions are performed continuously and summed up in an overall size distribution.

### Example: DLS flow mode for high resolution size distribution measurement of Bovine Serum Albumin [3]

Proteins are often very sensitive when isolated from living organisms for structural and functional analysis. They tend to alteration due to conformational changes resulting in dimerization, oligomerization or even polymerization and can therefore exhibit a polydisperse appearance. For polydisperse proteins, the DLS flow mode provides a much higher size resolution than batch mode DLS analysis to separate individual components.

BSA (5 mg/ml in PBS buffer) was used as model protein to be analysed by BeNano DLS flow mode utilizing a 27  $\mu$ l low-volume flow cuvette. Injection (100  $\mu$ l BSA solution) and separation were performed through a front-end SEC (mobile phase: PBS buffer, flow rate: 0.4 ml/min) with an RI detector. Subsequently, individual separated components entered the BeNano for size measurement under 25°C.

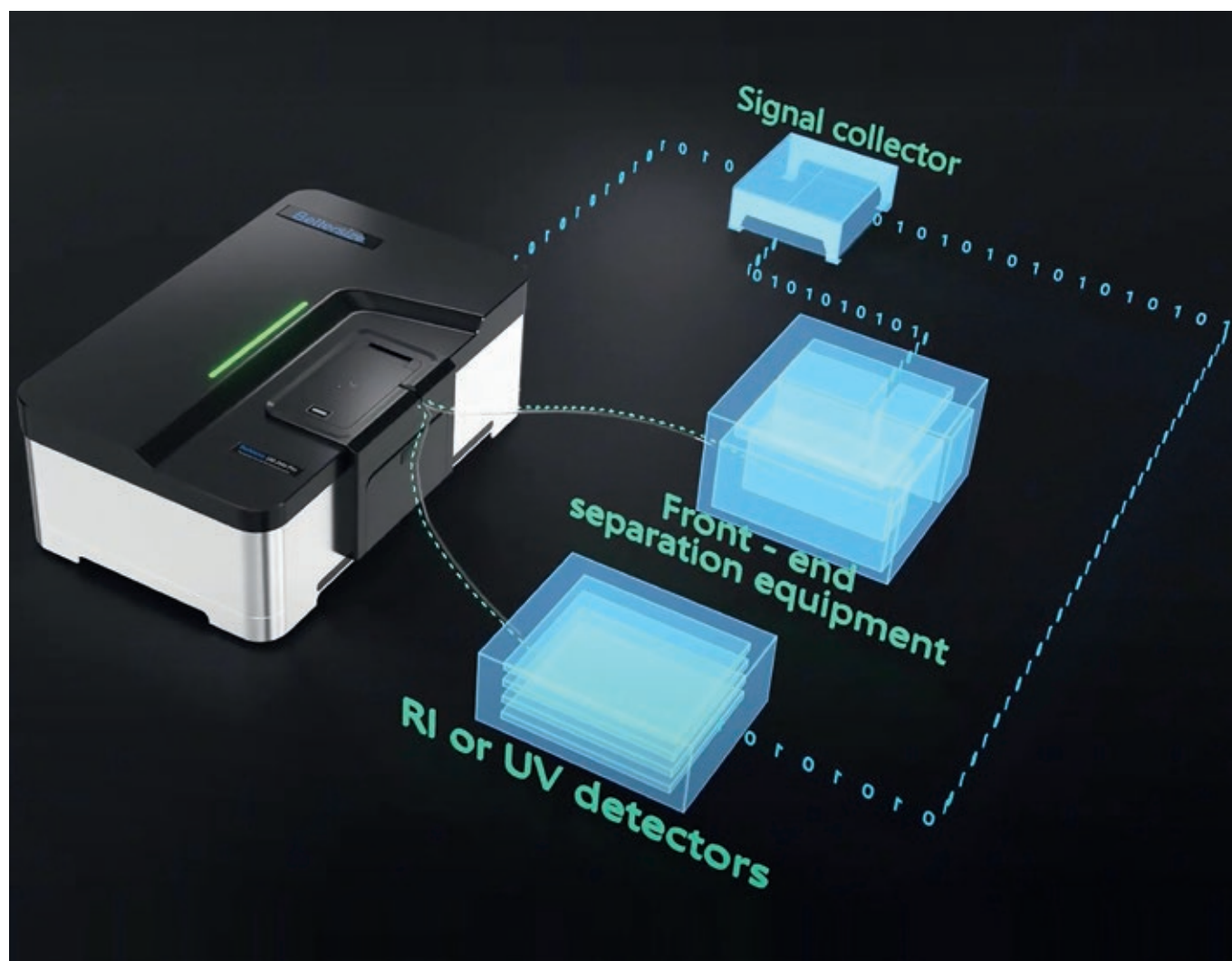


Figure 5 BeNano series DLS flow mode with front end separation equipment

The effluent curves are shown in Fig. 6. They show multiple peaks for BSA in PBS buffer. The peaks at around 6 ml represent BSA aggregates, peaks between 8-10 ml represent separated oligomers. The final major peak at around 10.5 ml represents the monomer of BSA. The larger area of the major peak indicates that the majority of the protein exists as monomers. The decreasing particle sizes detected in the size effluent curve (red dots) correspond well with the principles of SEC separation. This confirms the effectiveness of the front-end SEC in sample separation and validates the BeNano as a detector, effectively obtaining particle size information for each effluent component.

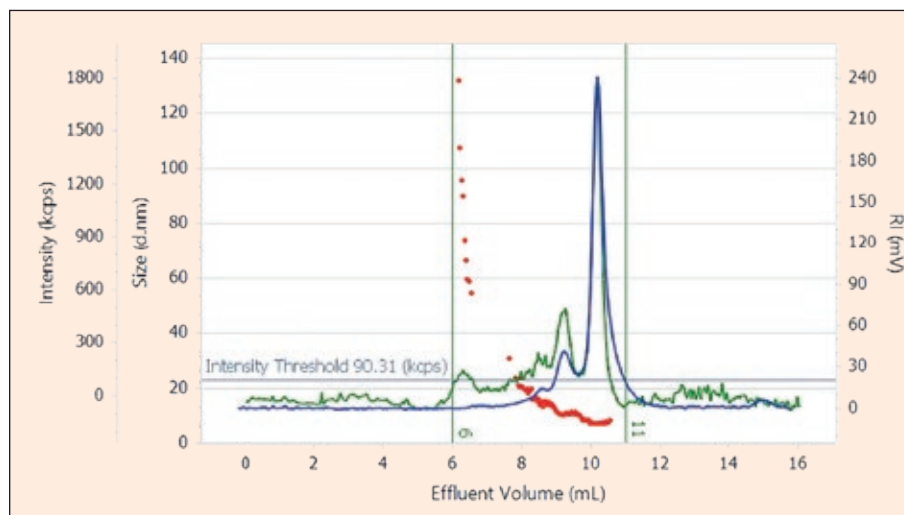


Figure 6 Intensity, RI and Size effluent curves of BSA (5% in PBS) – BeNano 180 Zeta Pro DLS flow mode

In Fig. 7 the chromatographic effluent curve is converted into an intensity weighted distribution curve and compared to batch mode BSA analysis. Batch mode detection only reveals two peaks, one at around 10 nm for monomers, dimers, trimers and oligomers in combination, and another at around 100 nm for larger aggregates. In contrast, applying DLS flow mode, different oligomeric and different aggregated BSA fractions can be distinguished besides the monomeric protein fraction at 7.21 nm. This clearly demonstrates, that the BeNano DLS flow mode can successfully distinguish oligomer components with very small size differences within the small size peaks and therefore enhances protein analysis in structural and functional analysis.

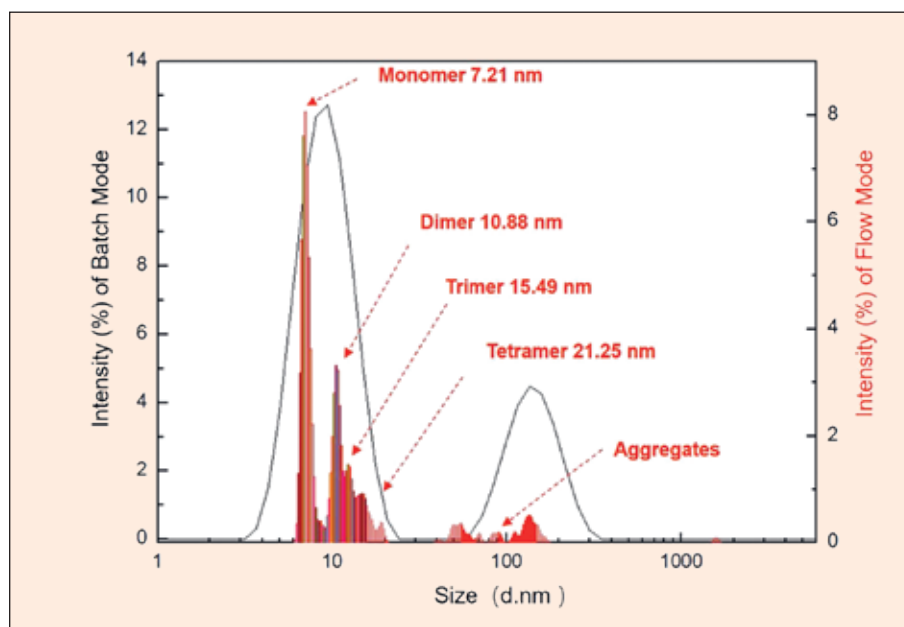


Figure 7 Intensity distribution curves of BSA (5 mg/ml in PBS) in batch mode (line chart) and flow mode (bar chart) – BeNano 180 Zeta Pro

## Summary

Instruments of the BeNano series are a helpful tool in comprehensive biomolecules' analysis. The flagship of the equipment series, the BeNano 180 Zeta Pro, combines dynamic light scattering (DLS) for particle size measurement, electrophoretic light scattering (ELS) for zeta potential determination and static light scattering (SLS) for molecular mass determination in one system. For both, in research and development as well as in quality control, all parameters are essential in protein structural analysis during processes e.g. enrichment, (scaling-up) production or storage. In addition, using tracer particles in DLS, the parameter portfolio is now expanded by microrheological characteristics, like complex viscosity, which help in stability analysis of protein solutions to detect alterations due to protein denaturation and aggregation. Besides these parameters already available, DLS particle size analysis by the BeNano is further improved upon by

the newly implemented DLS flow mode option, when equipped with a front-end separation system. This enables the separation of different oligomeric protein fractions. In contrast to classical DLS batch mode analysis, oligomeric protein fractions can then be detected individually by the BeNano. The identification of conformational differences of a protein is important in structural, functional and stability analysis of proteins.

## References

- [1] Particle World 23, 3P Instruments, [https://www.3p-instruments.com/wp-content/uploads/2022/09/PW23\\_engl\\_300dpi.pdf](https://www.3p-instruments.com/wp-content/uploads/2022/09/PW23_engl_300dpi.pdf)
- [2] Particle World 24, 3P Instruments, [https://www.3p-instruments.com/wp-content/uploads/2023/08/PW24\\_engl\\_300dpi.pdf](https://www.3p-instruments.com/wp-content/uploads/2023/08/PW24_engl_300dpi.pdf)
- [3] Guo, Z., Ning, H.: Utilizing DLS Flow Mode for High-resolution Size Distribution Measurement of BSA, Bettersize Application Note

# BeScan Lab

## The new benchmark in stability analysis

Dr. Christian Oetzel, christian.oetzel@3P-instruments.com



Figure 1 BeScan Lab

- Stability analysis of suspensions and emulsions in real-time
- Static multiple light scattering technology (SMLS)
- Transparent and opaque dispersions - measurement in transmission and backscattering
- Flocculation, Creaming and Sedimentation detection
- Determination of the Instability Index  $I_{US}$

### Introduction

BeScan is the name of the new stability analyzer based on static multiple light scattering (SMLS) technology. It is predestined to detect destabilization processes such as framing, agglomeration, sedimentation and coalescence at the earliest stages. The time and spatially resolved detection of transmission and backscattering allows analysis of dilute and concentrated suspensions and emulsions (up to 95% v/v) as well as foams. Temperature-dependent measurements up to 80°C are possible. The instability index  $I_{US}$  is determined as a process parameter for direct comparison of the stability of similar formulations.



Figure 2 BeScan Lab with sample

### Key Benefits

#### True stability measurement:

- Measurement is carried out without applying any mechanical or external stress
- Test is non-destructive without direct contact to dispersion

#### Characterization of the original sample:

- Analysis of translucent and highly concentrated systems in its original state without any dilution (0 to 95% v/v)
- Wide range of size (10 nm to 1 mm)

#### Identification and quantification of destabilization mechanisms:

- Easy identification and quantification of various destabilization effects like creaming, sedimentation, flocculation, coalescence, and breaking
- Quantification of destabilization by kinetic parameters and destabilization index

#### Fast detection of destabilization:

- Data acquisition with a resolution of 20  $\mu\text{m}$  enables quicker observation of sample stability than with the naked eye
- Precise temperature control up to 80°C to accelerate unstable phenomena
- "One-to-many" system enables simultaneous testing of different samples with one software

## Measurement principle

The BeScan uses Static Multiple Light Scattering (SMLS) to record particle agglomeration and migration in liquid dispersions. A probe head which is equipped with a laser light source and two detectors (0° and 135°) moves vertically over the measuring cell, which is filled with the sample. During the movement, a transmission signal (0° - for transparent, diluted samples) and backscatter signal (135° - for concentrated opaque samples) are recorded continuously every 20 µm over the entire sample height. Both signals are related to particle size and concentration and its change over time indicates destabilization of the sample. Following each scan, an instability index ( $I_{US}$ ) can be computed. Short-term or Long-term stability can then be assessed based on the trend of  $I_{US}$ .

$$I_{US} = \sum_n \frac{\sum_h |I_n(h) - I_{n-1}(h)|}{H}$$

In addition, the mean particle size can be determined by analyzing the transmission, backscattering or particle migration rate.

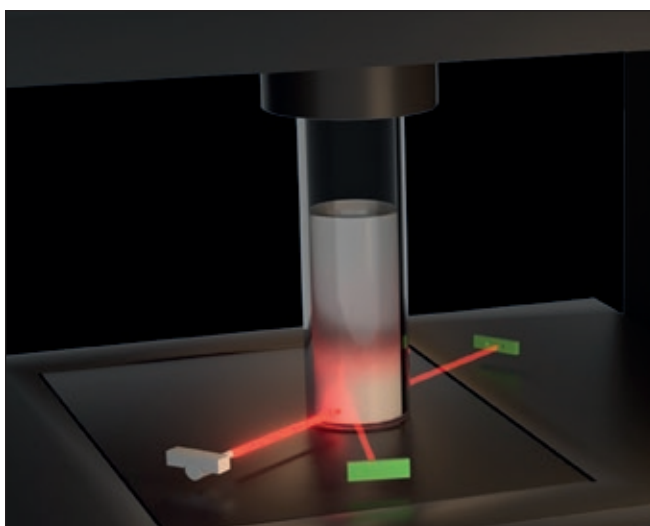


Figure 3 Probe head

Table 1 Specifications

Parameters	Values
Measurement principle	Static Multiple Light Scattering (SMLS)
Detection angle	0° transmission and 135° backscattering
Light source	850 nm LED
Scan step	20 µm
Maximum volume fraction	95%
Measurement range of particle size	0.01 - 1000 µm
Temperature range	RT+5 °C - 80 °C (±0.5 °C)
Sample volume	4 - 25 mL
Measurement mode	Regular/Fixed point/Temp. trend
Dimension	460(L) x 260(W) x 280(H) mm
Weight	13.5 kg
Power	AC100 - 240 V, 50 - 60 Hz, 3.8 A
ISO compliance	ISO/TR 18811:2018, ISO/TR 13097:2013 ISO/TR 21357:2022, ISO/TS 22107:2021

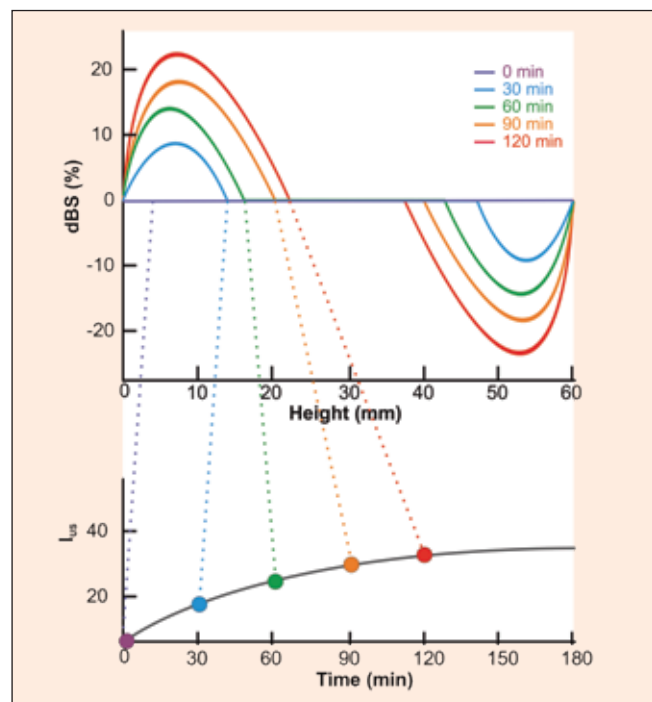
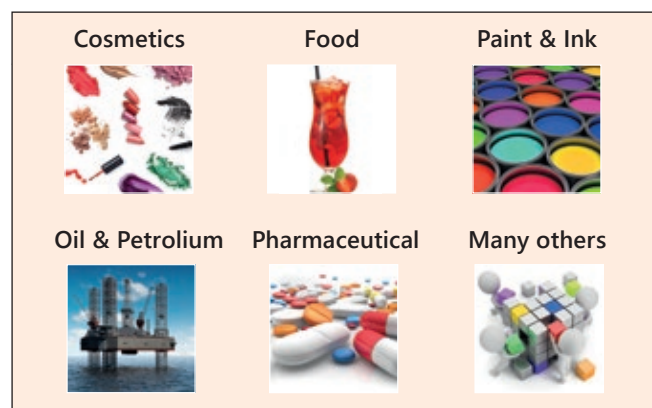


Figure 4 Principle BeScan measurement

## Applications



## News



### 3P prep 800 - sample preparation unit for various BET instruments

The 3P prep 800 degassing device has eight stations for sample preparation for physisorption measurement of the specific surface area of BET and the pore size distribution. Sample preparation can be carried out both in a vacuum and in flow-through mode. The stations are divided into two separate degassing parts, each with 4 stations quipped to their own vacuum meter and valve control. The samples are degassed in a temperature-controlled heat zone up to 400 °C with the option of temperature ramps. The samples cool down in a storage zone with active airflow cooling. You are welcome to contact [info@3p-instruments.com](mailto:info@3p-instruments.com) to check whether this sample preparation station with an excellent price-performance ratio is also compatible with your type of measuring cell - 3P Instruments offers various options for this.

### New events like webinars you find here

[www.3p-instruments.com/events/](http://www.3p-instruments.com/events/) and feel free to contact [info@3p-instruments.com](mailto:info@3p-instruments.com) for request of special training program or other ways to benefit from our experience and our lab capabilities.



### Altamira Microreactor Systems

Altamira Instruments is a supplier of chemisorption instrumentation as well as bench-scale microreactor systems for industrial and research use. AMI instruments have been installed at more than 300 locations around the world. Among these installations are leading national laboratories, influential academic catalyst research groups and major chemical research centers.

Altamira offers a variety of custom designed and fully automated chemisorption and physisorption analyzers and reactor systems. From instruments that conduct temperature-programmed characterization (TPR/TPO/TPD) to micro-reactors designed for a specific chemical process to surface area analyzers, Altamira can provide the instrument solution to your laboratory needs.

Contact [info@3p-instruments.com](mailto:info@3p-instruments.com) to get more information and to come to direct contact to the specialists to discuss your specific application.

### Latest news at the time of going to press: 3P will be offering a range of devices for thermal analysis in the future!

3P Instruments will soon be offering a complete range of thermal analysers with a wide operating temperature range. This range consists of DSC, PDSC, DTA, TGA, TMA and STA analysers with temperature ranges from -125 °C to 1500 °C. Simple operation combined with advanced analysis functions – in case of interest please send 'thermal analyser' to [info@3p-instruments.com](mailto:info@3p-instruments.com) for some overview information.



## The new BetterPyc 380 gas pycnometer

The BetterPyc 380 is an automatic gas pycnometer that uses the gas displacement method to deliver highly accurate measurements with ease, offering precision at its best. With temperature control, pressure sensing, and intuitive software, it measures the volume, true density, solid content, and open cell content of your samples with up to 4-digit accuracy. Designed for research and production in a wide range of industries, the BetterPyc 380 will unlock the full potential of your products.

Contact [info@3P-instruments.com](mailto:info@3P-instruments.com) to get more information.



## No news, but still up to date:

3P Instruments as former Quantachrome GmbH continues to offer service and maintenance for the CILAS and Quantachrome devices, installed by us over the last decades. We not only have the technicians available with many years of the relevant software and hardware experience, but also the company philosophy to help our customers with their instruments so long there are spare parts available. Rest assured that most spare parts and consumables are still available, most devices can be repaired by 3P Instruments, and an enquiry can simply be sent to [info@3P-Instruments.com](mailto:info@3P-Instruments.com)

**Replacement and spare parts catalog NOVA 1000e-4200e**

**3P INSTRUMENTS** Characterization of particles · powders · pores

Item number	Description	Comments
<b>Measuring cells (Standard)</b>		
90303	Measuring cell 6 mm, long	Long Sample Cells "long" = 200-250 mm 6, 9 and 12 mm corresponds to the outside pore diameter
90309	Measuring cell 6 mm, small bulb (25 mm), long	
90319	Measuring cell 6 mm, large bulb (25 mm), long	
90318	Measuring cell 9 mm, long	
90313	Measuring cell 9 mm, small bulb (25 mm), long	
90317	Measuring cell 9 mm, large bulb (25 mm), long	
90326	Measuring cell 12 mm, long	Short Sample Cells "short" = 145-155 mm
90321	Measuring cell 12 mm, small bulb (25 mm), long	
90328	Measuring cell 12 mm, large bulb (25 mm), long	
<b>NOVA-S</b>		
90310	Measuring cell 6 mm, short	Short Sample Cells "short" = 145-155 mm
90312	Measuring cell 6 mm, small bulb (25 mm), short	
90320	Measuring cell 6 mm, large bulb (25 mm), short	
90316	Measuring cell 9 mm, short	
90315	Measuring cell 9 mm, small bulb (25 mm), short	
90318	Measuring cell 9 mm, large bulb (25 mm), short	
90329	Measuring cell 12 mm, short	
90323	Measuring cell 12 mm, small bulb (25 mm), short	
90330	Measuring cell 12 mm, large bulb (25 mm), short	

## The Ultimate DSC and Ultimate micro calorimeter UMC

The **Ultimate DSC's** revolutionary sensor is based on patents from one of the most prestigious DSC research laboratories. Its remarkable and unmatched performance makes it the most sensitive device on the market. These allow the Ultimate DSC to measure energy transitions as small as protein denaturation with minimal amounts of sample. A real revolution in the DSC market with unique advantages:

- Low sample volume required (5-100µl)
- No cleaning procedure
- High scan rate (up to 10°C/min)
- High concentration solution studies
- Solid and gel studies
- Easy to automate

More information with video "How to prepare an experiment with the Ultimate DSC" is to find at [www.calneos.com/en/ultimate-dsc-en/](http://www.calneos.com/en/ultimate-dsc-en/)

The **Ultimate micro calorimeter UMC** is a differential temperature scanning micro calorimeter offering unrivalled sensitivity, enabling the study of all types of materials, including the most dilute solutions. It operates as a conventional microcalorimeter. The UMC's unique, innovative design enables sensitive measurement at a level never achieved before for a micro calorimeter with extractable cells/test crucibles:

- Wide temperature range
- Cells adapted to your applications
- Interchangeable sensor
- Unrivalled accuracy and sensitivity

For more information, please contact [info@3P-instruments.com](mailto:info@3P-instruments.com) or [www.calneos.com](http://www.calneos.com)





# Studies on the optimal characterization of smallest portions of porous structures

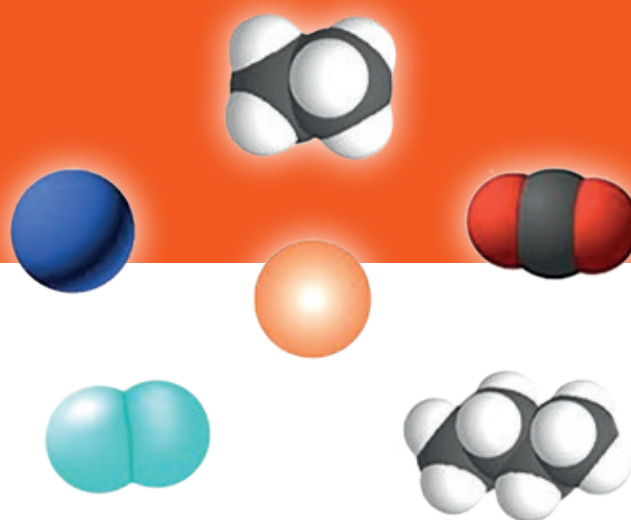
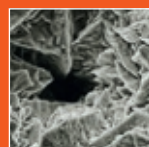
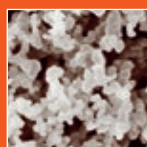
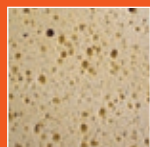
Sebastian Ehrling, [sebastian.ehrling@3P-instruments.com](mailto:sebastian.ehrling@3P-instruments.com)



Funded by the European Union



This project is co-financed from state funds on the basis of the budget adopted by the Saxon state parliament



## Introduction

Not only the IUPAC recommends the use of argon at 87 K instead of nitrogen near 78 K for the characterization of porous materials [1], also the ISO 9277 [2] describes problems when using the BET method for the determination by the use of the  $N_2$ . So, regardless of the fact that  $N_2$  interaction problems with a material surface can influence pore volumes, specific area and pore size distribution results,  $N_2$  near 78 K is still the most common technique due to the availability of liquid nitrogen for reasons of comparison. However, this is only true for samples with a certain accessible pore volume under the appropriate measurement conditions. When it comes to samples with narrow ultramicropores or a very small surface area and almost no pore volume, such as thin films or non-porous samples  $N_2$  and Ar reach their limits. At cryogenic temperatures, both  $N_2$  (77.35 K) and Ar (87.3 K) can reach a saturation pressure of 101.3 kPa. However, if the surface area of the sample is very small and thus the number of adsorbed gas molecules on the sample is very little, only a minor change in the measured pressure of the sample gas is caused.

To overcome such phenomena, the free space and the amount of free gas molecules need to be reduced. There are several possibilities for reducing the free space in the sample cell and with that enhancing the selectivity.

- Optimized sample cells e.g. smaller bulb or no bulb
- Use of filling rods (remark: the use of a filler rod is only recommended when no micropore analysis is performed, because the thermal transpiration correction is based on the mean free path length of the measuring cell without a glass rod)
- Use of a small manifold (dosing volume)
- Separation of the dosing volume from the sample cell volume
- Minimizing the cold zone volume

If the free space volume is optimized, a minimum of  $1 \text{ m}^2$  of absolute sample surface must be available in the cell for  $N_2@78\text{K}$  or  $\text{Ar}@87\text{K}$  adsorption regardless of the measuring error which at

that limit can be already quite large. Another approach is the reduction of the saturation pressure. With a reduction of the saturation pressure of adsorptives, the pressure range for BET and pore size calculations is reduced significantly, which results in a sensitivity enhancement of the sorption device [7].

## Krypton at cryogenic temperatures

IUPAC recommends the use of krypton near 78 K. The reason for this is the drastic reduction in vapor pressure. This can be shown very well using a calculation example. We assumed a sample with an absolute surface area of  $1 \text{ m}^2$  and a sample cell volume of  $20 \text{ cm}^3$ . At a relative pressure  $p/p_0$  of 0.2, the amounts adsorbed were calculated for  $N_2$  and Kr and equal:

- $N_2 = 0.287 \text{ cm}^3$
- $\text{Kr} = 0.222 \text{ cm}^3$

The volume of gas remaining in the sample cell under standard temperature and pressure (STP) conditions was calculated using the following equations:

- $$V_{N_2} = 20 \text{ cm}^3 \frac{101.3 \text{ kPa} \cdot 0.2}{101.3 \text{ kPa}} \cdot \frac{273 \text{ K}}{77 \text{ K}} = 14.14 \text{ cm}^3$$
- $$V_{\text{Kr}} = 20 \text{ cm}^3 \frac{0.35 \text{ kPa} \cdot 0.2}{101.3 \text{ kPa}} \cdot \frac{273 \text{ K}}{77 \text{ K}} = 0.046 \text{ cm}^3$$

By combining the amount adsorbed with the gas remaining in the sample cell, we obtained the total dosing volumes:

- $N_2: 0.287 \text{ cm}^3 + 14.14 \text{ cm}^3 = 14.431 \text{ cm}^3$
- $\text{Kr}: 0.222 \text{ cm}^3 + 0.046 \text{ cm}^3 = 0.268 \text{ cm}^3$

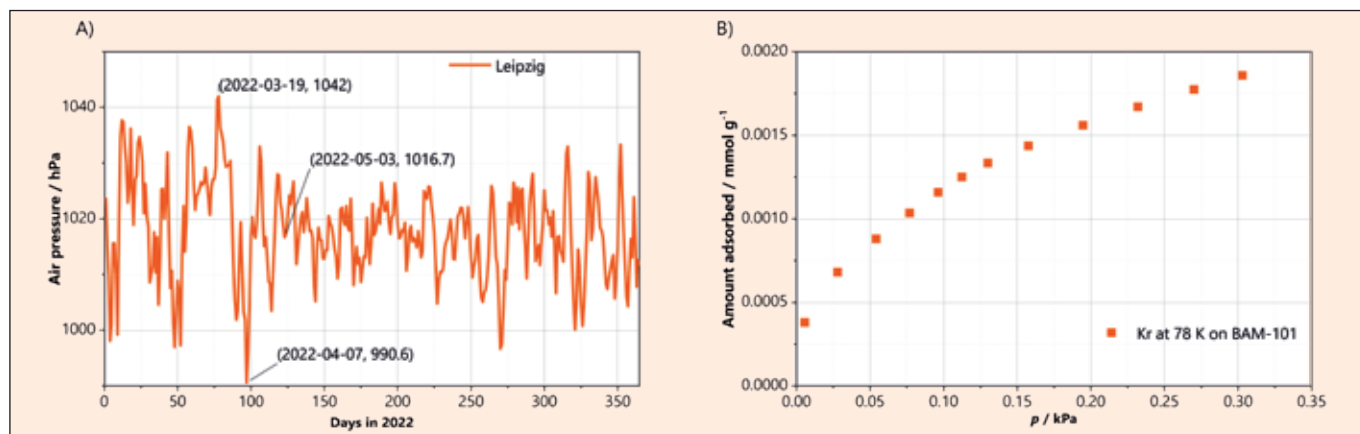


Figure 1a Ambient air pressures in Leipzig in 2022

Figure 1b Krypton isotherm at 78 K on BAM-101

From these values, we calculated the percentage of non-adsorbed molecules, which are around 98 % for N<sub>2</sub> and 17 % for Kr respectively. In other words, this means that the adsorption of Kr results in much greater relative pressure changes, which increases the sensitivity of the measurement and allows even the smallest absolute surface areas to be determined.

However, in contrast to N<sub>2</sub> near 78 K and Ar near 87 K a measurement of the p<sub>0</sub>-value of the Kr-adsorptive during the experiment is not possible. And with that a p<sub>0</sub> correction due to temperature changes of liquid nitrogen or argon coolant during the measurements is not known for standard krypton measurements around 78 K or 87 K. This is due to the fact that both temperatures are below the triple point of Kr and therefore, according to the phase diagram, there is no transition between the gas phase and the liquid phase. Similar to CO<sub>2</sub> at 195 K, a transition from the gas phase to a liquid-like phase of krypton takes place within pores of a certain size. However, the pressure of this phase cannot be measured and can only be obtained by extrapolating the existing vapor pressure curve. The IUPAC defines a value of 2.63 Torr or 0.35 kPa, but does not specify where this value comes from.

### Vapor-pressure curve of krypton

A literature search showed that Meihuizen and Crommelin [3] described in their publication from 1937 a vapor pressure curve of krypton. To achieve this, they utilized p-T value pairs above the triple point of Krypton and extrapolated them to access vapor pressures of liquid krypton below the triple point. For the fitting process, they employed a formula that later became known as the Riedel equation [4]. The equation is in the form:

$$\log_{10} p = \frac{A}{T} + B \cdot \log_{10} T + C \cdot T + D \quad (1)$$

Table 1 Parameter of Riedel-like equation for different data sets

Parameter	Data from [3]	coolProp 116-209 K	coolProp 116-135 K
A	- 899.979	- 894.60004	- 1185.93449
B	- 12.554	- 12.57883	- 24.79723
C	0.0175105	0.01778	0.04117
D	31.50311	33.48762	58.51538
p <sub>0</sub> @77.4 K / Torr	2.514	2.646	2.626

Regardless, in the literature, a p<sub>0</sub> value for liquid Krypton at 77.4 K of 2.63 Torr (0.35064 kPa) has been established [5]. However, when Equation (1) is used with the corresponding parameters (Table 1, column 2) to calculate the pressure at 77.4 K, a value of 2.514 Torr (0.33517 kPa) is obtained.

Therefore, the equation from 1937 was optimized based on the vapor pressure data from the coolProp database [6]. Additionally, the established value of 2.63 Torr at 77.4 K was included as another data point. A summary of the parameters is provided in Table 1. It is evident that when the entire temperature range of the coolProp database is used for the fit, the curve exhibits only moderate agreement in the extrapolated region. Consequently, only data points below 135 K were used for the fit, sacrificing accuracy in the upper temperature range for higher precision below the triple point.

Our recommendation is that below the triple point, the adjusted Riedel-like equation should be used. For temperatures above the triple point, access to the coolProp database should be utilized. Although there is now an equation that very precisely matches the recommended p<sub>0</sub> value of krypton at 77.4 K, there is still the problem that this value only applies exactly for 77.4 K. The smallest variations in the purity of the liquid nitrogen, changes in air pressure and humidity influence the temperature of the liquid nitrogen and thus the vapor pressure of the liquid-like phase of krypton. As an example, changes in air pressure in Leipzig over a few weeks can be read from Figure 1a.

With other words, also the boiling temperature of liquid nitrogen deviates between 77.15 and 77.58 K. The influence of air pressure becomes even clearer when an isotherm that has been measured is evaluated fictitiously with different air pressures. For this purpose, the standard material BAM-101 was measured with krypton at a temperature of 78 K (Figure 1b) and the surface area was determined using the BET equation (Table 2).

**Table 2** Temperature and pressure fluctuations and resulting surface areas of BAM-101

Air pressure / hPa	T <sub>LN2</sub> / K	P <sub>0*, Kr</sub> / kPa	SA <sub>BET</sub> / m <sup>2</sup> g <sup>-1</sup>
1042	77.58	0.371	0.173
990.6	77.15	0.335	0.164
1016.7	77.38	0.355	0.169
irrelevant	78	0.4053	0.177

Subsequently, based on the air pressure, fictitious  $p_0$  values were used for the evaluation. The results show that solely due to the fluctuation of the air pressure an error of about 5 % occurs in the evaluation of the data. In addition to the vapor pressure, the liquid density and the resulting spatial requirement of each adsorptive are also temperature-dependent. This clearly shows that a control of the temperature, especially for measurements where the vapor pressure cannot be determined experimentally, is essential for a reproducible and reliable measurement. 3P Instruments has therefore extended its cryoTune portfolio to reliably control the measurement environment near the boiling point of liquid nitrogen.

## Technical aspects of the new cryoTune 77

The fourth cryoTune model within this series completes the temperature range from 77 K or the boiling point of liquid nitrogen up to 323 K or room temperature (Figure 2). Due to these innovations, almost all adsorptives can be measured with a large temperature constancy (deviation < 0.004 K).

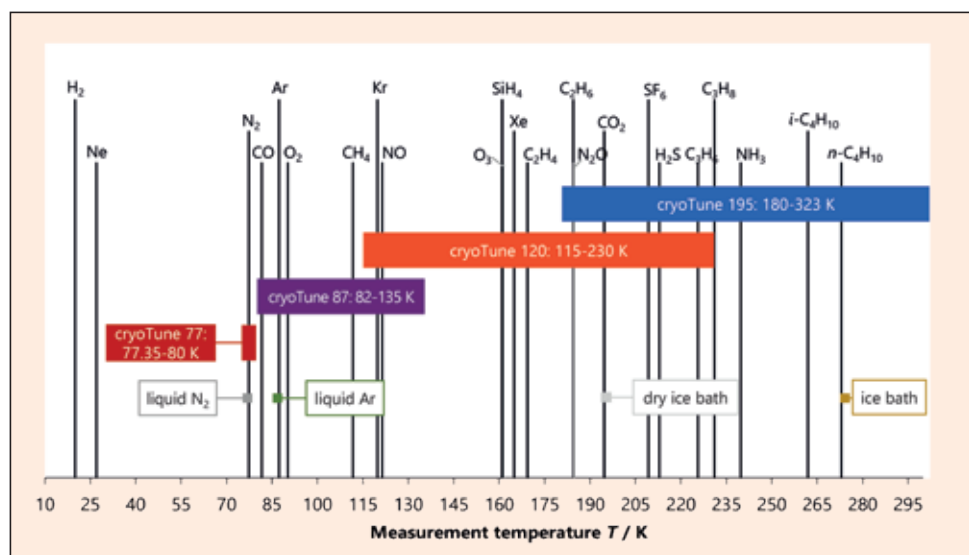
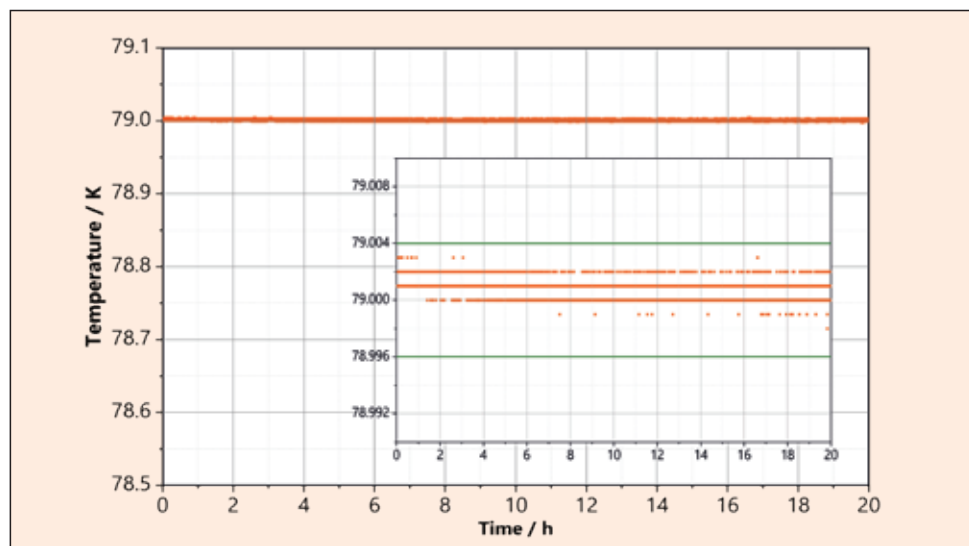
The principle of operation of the cryoTune 77 is analogous to the already known versions cryoTune 87, cryoTune 120 and cryoTune 195. Only small changes in the structure and design of the cryoTune allow the temperature range of 77.35 K - 80 K to be achieved. Due to these changes and the fact that it operates just

above the boiling point of liquid nitrogen, the service time is somewhat shorter compared to the other models. However, at 79 K, this is still 20 hours (Fig. 3). At lower temperatures such as 78 K or 77.5 K, the life time is correspondingly longer.

## Alternatives and Outlook

In addition to the numerous advantages of krypton listed above, especially in comparison with N<sub>2</sub>, there are also some disadvantages. The costs of krypton gas, the mandatory presence of a turbo-pump and low-pressure sensors (1 Torr and 10 Torr) are particularly noteworthy. However, the greatest uncertainty certainly stems from the fact that no  $p_0$  can be measured. The values used for the vapor pressure of the liquid-like phase are solely based on an extrapolation of the vapor pressure curve above the triple point.

Following the logic of the sorption method sensitivity factor (SMSF) [7] to gas sorption measurements and based on the fact that practically any temperature between 77.5 and 323 K can be set using the various cryogenic units, further adsorptives can be considered for the observation

**Figure 2** The cryoTune portfolio of 3P Instruments**Figure 3** Temperature stability test at 79 K for 20 hours with the cryoTune 77

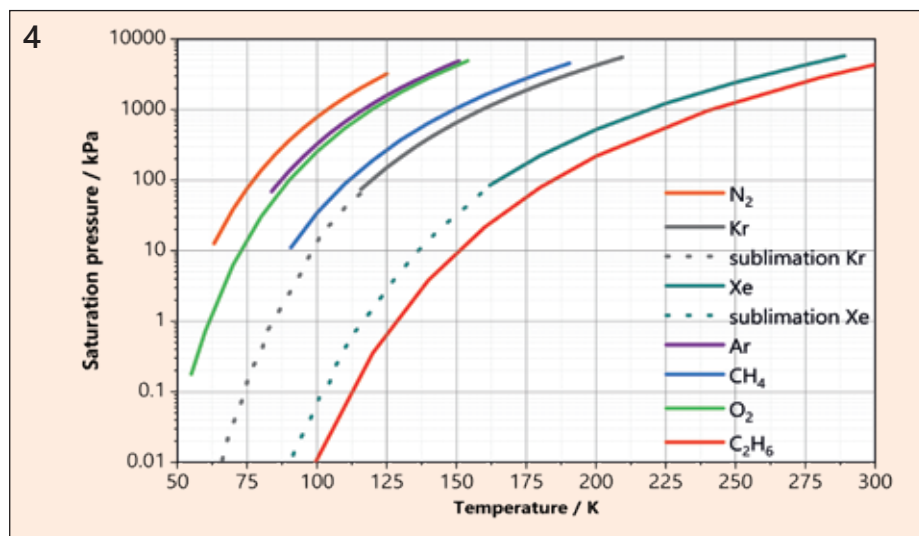


Figure 4 Vapor pressure curves of different gases. The dotted lines represent the extrapolation curves of the vapor pressure curves below the triple point

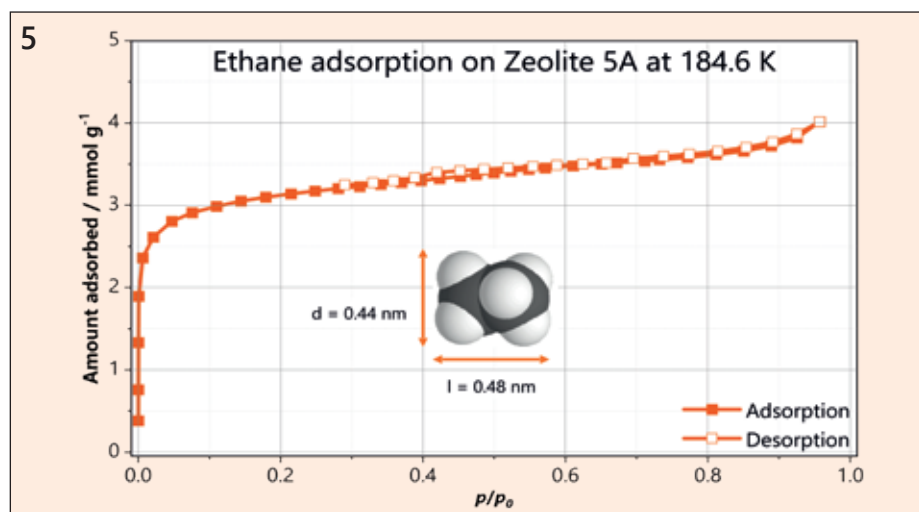








Figure 5 Ethane adsorption on Zeolite 5A at the boiling point of ethane at 184.6 K. Inlet: Dimension of the slightly elongated ethane molecule

### Adsorptives with critical molecule diameter (nm)

	CO <sub>2</sub>	0.28
	N <sub>2</sub>	0.30
	Ar	0.34
	Kr	0.36
	C <sub>2</sub> H <sub>6</sub>	0.44
	C <sub>4</sub> H <sub>10</sub>	0.49

of the smallest surfaces. A look at the vapor pressure curves of various gases (Figure 4) shows possible alternatives. If a  $p_0$  of 10 kPa is aimed for and thus an increase in sensitivity by a factor of 10 over Ar@87 K or N<sub>2</sub>@78 K, the following examples of N<sub>2</sub>@63 K, O<sub>2</sub>@73 K or CH<sub>4</sub>@91 K, for example, come to mind. However, the first two mentioned are excluded from our considerations, as a helium cryostat is required to reach these temperatures and simple and cost-effective handling is impossible. CH<sub>4</sub> has a certain potential, but here it is only necessary to measure just above the triple point to achieve a  $p_0$  of 12.2 kPa. Longer-chain hydrocarbons such as ethane, propane or butane, however, have a very large transition range from the gaseous to the liquid phase, i.e. they have a pronounced vapor pressure curve.

Based on initial tests, ethane was classified as very promising. The molecule has similar dimensions to the nitrogen molecule, but has a lower quadrupole moment (0.65 vs 1.52 / 1026 esu cm<sup>2</sup>). As a result, weaker interactions with polar surfaces are to be expected compared to N<sub>2</sub>. However, the adsorption temperature in particular, which is over 100 K higher ( $T_b$ , N<sub>2</sub> = 77.4 K vs  $T_b$ , C<sub>2</sub>H<sub>6</sub> = 184.6 K), reduces kinetic influences enormously, as can be seen from the example of zeolite 5A in Figure 5.

Interestingly the fact that vapor pressures lower than 0.35 kPa (benchmark of Kr at 77.4 K, IUPAC recommendation) can only be achieved by lowering the adsorption temperature. It must also

be noted that at such low pressures, high demands are placed on the measuring device. Particular attention must be paid to extremely high seal integrity, as the lowest leak rates will have a very strong influence on the result. In addition, the pressure sensors installed must work very accurately at low pressures and the dosing unit has to meet high demands. We would like to tackle all of these issues together with the Institute of Nonclassical Chemistry in Leipzig/Germany (INC) over the next few years to find solutions within the EU-funding project to develop the basis for a new practicable method to characterize smallest porous quantities in the pore size range of 0.5 – 500 nm.

### References

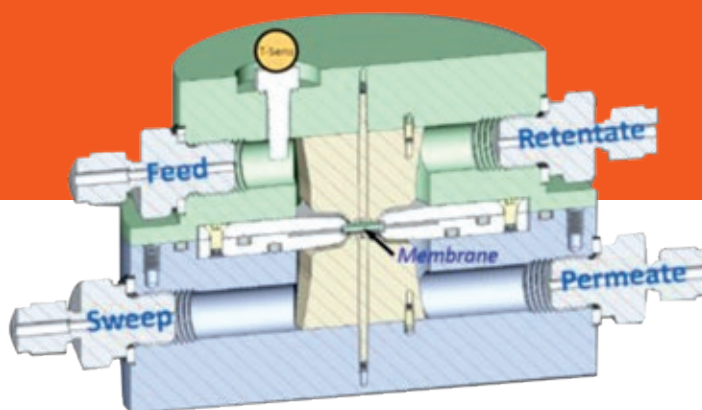
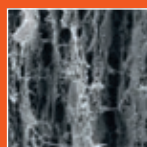
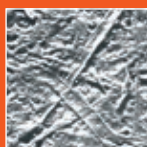
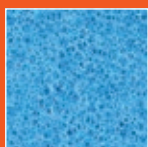
- [1] IUPAC Technical report, Pure Appl. Chem. 87(9-10), 1051-1069 (2015)
- [2] ISO 9277:2010: Determination of the specific surface area of solids by gas adsorption - BET method
- [3] J. J. Meihuizen, C. A. Crommelin, Vapour pressures of liquid krypton, Physica 4.1 (1937): 1-4
- [4] L. Riedel, Neue Dampfdruckformel, Chem. Eng. Tech. 26 (1954) 83–89
- [5] C. Reid, J. M. Prausnitz, B. E. Poling, The properties of gases and liquids, McGraw-Hill, New York, 1987
- [6] I. J. Wronski, S. Quoilin, V. Lemort, Pure and Pseudo-pure Fluid Thermophysical Property Evaluation and the Open-Source Thermophysical Property Library CoolProp, Ind. Eng. Chem. Res. 2014, 53, 6, 2498–2508
- [7] D. Klank, S. Ehrling, 3P Instruments, Particle World 24, p.15 - 18

# Development of a comprehensive measurement system for membrane separation properties

Matthias Graf<sup>1</sup>, Marcus Lange<sup>2</sup>, Jens Möllmer<sup>2</sup>, Sebastian Ehrling<sup>1</sup>

matthias.graf@3P-instruments.com, lange@inc.uni-leipzig.de

1: 3P Instruments, 2: INC Leipzig



## Introduction

In many areas of the chemical industry, food or medical technology, methods are required to separate mixtures of substances or to detect the penetration of fluids through separation layers. In addition to classical sorption processes, membrane technology is often used to perform the separation of gas mixtures. It benefits from its modular design and optimal applicability, especially for small gas flows. The most important part of membrane technology is the membrane material itself, which can act either as a "sieve" (different pore sizes of the membrane act as a size selector) or via a solution diffusion mechanism (different molecules permeate the membrane at different rates). In this respect, gas permeation of single component gases (permeability) and eventual gas separation properties (selectivity, gas separation selectivity) are key metrics to evaluate the membrane's capability for many potential separation processes.

## Fundamentals of permeation measurements

The characterization of the separation performance of materials across a broad spectrum, from macroscale porous membranes to micron-scale thin barrier films, is traditionally accomplished by flow methods. The determination of permeation and separation is typically accomplished by three different approaches:

- Dead-end mode
- Cross-Flow mode
- Wicke-Kallenbach (WK) mode

The operation principles are shown in Figure 1. Amongst these, the dead-end mode is the simplest approach, as a feed gas stream enters a closed volume on one side of the membrane and the outflow on the other side (permeate side) is determined in terms of flow rate and composition while monitoring the pressure difference (Feed vs. Permeate). This method is particularly suitable for highly permeable membrane samples intended for the separation of gases with low levels of impurities.

In contrast, the cross-flow mode prevents a steady pressure increase on the feed side and avoids risks of membrane damage and time-dependent concentration gradients across the membrane by opening the feed side. Herein, the non-permeated gas (retentate) is allowed to flow out and the permeated gas is characterized as above. In addition, a pressure regulator can be added to the feed side to enable specific and constant feed pressures to be set and therefore determine permeability under static conditions.

In Wicke-Kallenbach (WK) mode, an additional gas flow (sweep) into the permeate part of the cell is added to the cross-flow principle. The sweep causes a flushing effect of the permeate gas to a) homogenize the concentration in the permeate

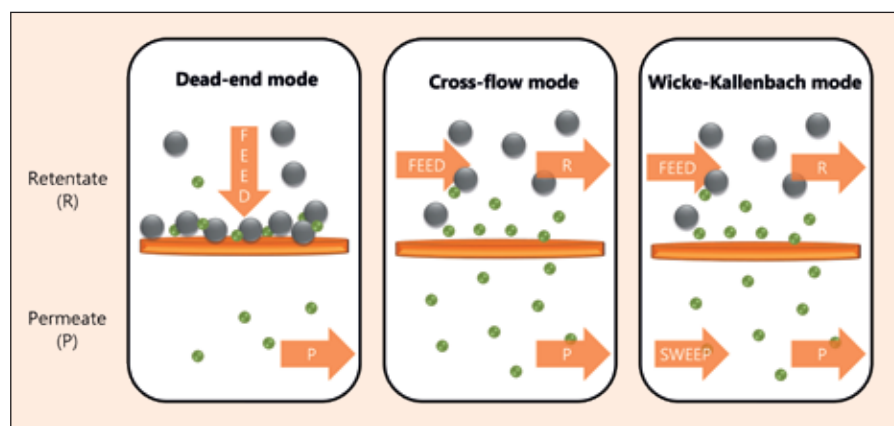
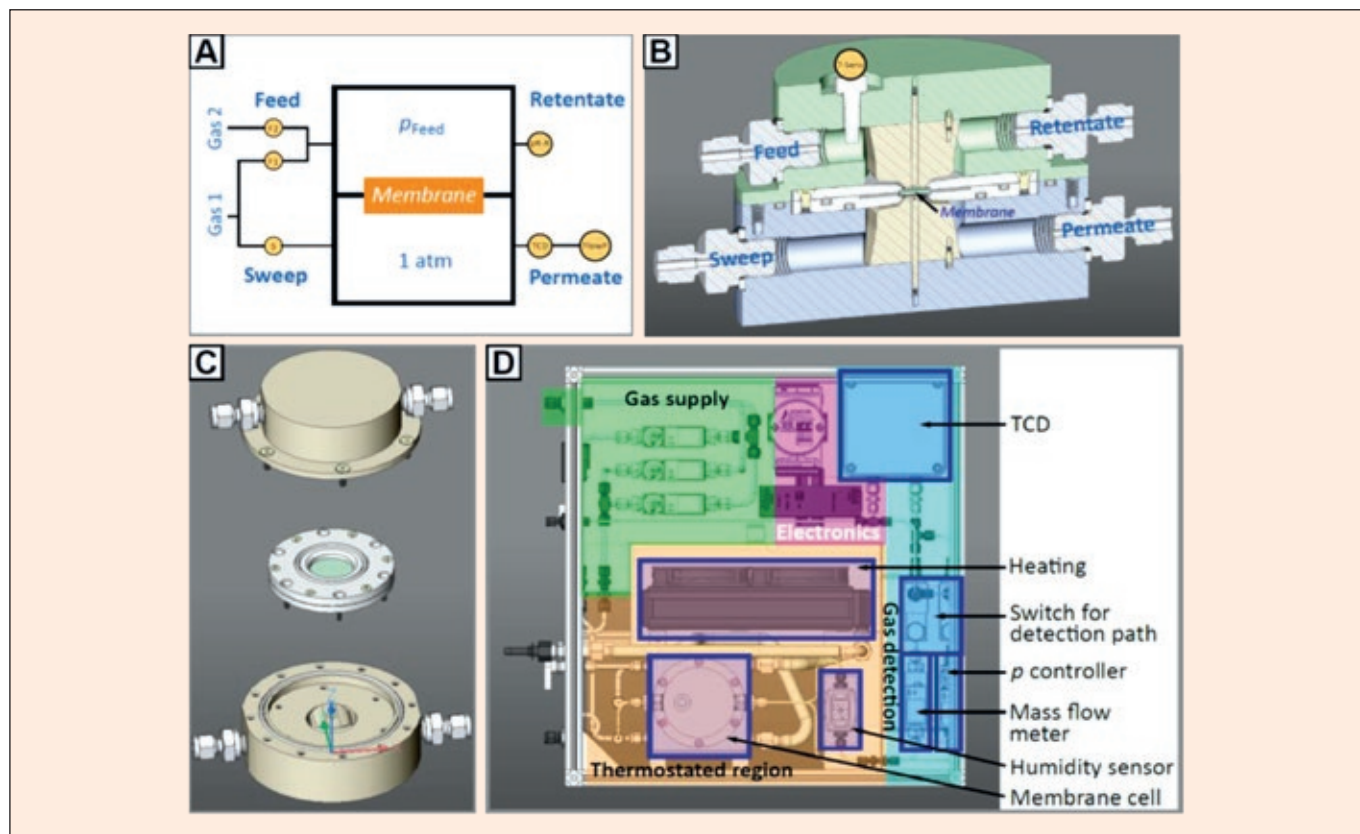


Figure 1 Three main operation principles of membrane characterization



**Figure 2** MOMT test setup

- A. Flow scheme feasible for operation under various modes (dead-end, cross-flow, Wicke-Kallenbach)
- B. Cross-sectional drawing of assembled membrane test cell with gas channels
- C. Explosion sketch of membrane test cell as during installation including a size-adaptable membrane holder
- D. Schematic top-view onto instrument with elementary components labelled

chamber and b) remove permeate gas from the membrane surface and regain initial conditions. As a result, the concentration gradients across the membrane remain constant and the permeate gas is diluted.

### The MOMT set-up

Figure 2A shows a flow scheme of the MOMT setup. It illustrates how the different measurement principles described above can be implemented:

In the dead-end approach, a defined feed gas (mixture) is adjusted by the mass flow controllers F1 and F2. The pressure controller on the retentate side (pR-R) is set to an infinitely high set pressure, to force the gas flow through the sample, while monitoring the actual pressure difference from feed and permeate. On the permeate side, zero sweep gas flow is set at the corresponding mass flow controller (S) and the permeate gas is monitored for composition (thermal conductivity detector, TCD) and flow (mass flow meter, FlowP).

The cross-flow mode is achieved by setting the pR-R either to zero pressure (free passage of feed gas) or to a defined pressure (e.g. for ceramic membranes within their crack tolerance).

This setup further transforms into the WK mode when a sweep flow is set at S. To enable quantitative measurements of permeate and retentate of mixed gases, the gas detection path can be switched by valves to either detect the composition of the permeate or the retentate.

The membrane cell itself is the heart of the entire MOMT setup and can be seen in Figure 2B. To adapt to different sample diameters, we have developed a sample holder for samples from 10 to 35 mm in diameter with an effective permeated diameter of 9 mm. For samples with lower permeability or/and if larger permeation areas are desired, this size can be increased up to 32 mm. Other sample thicknesses of 0.025 - 1 mm can be installed using PTFE spacers if necessary. For different geometries, special sample holders can be customized to fit the cell. In this regard, the MOMT approach is suitable for a wide

variety of potential sample geometries. In addition to this size flexibility, the sample holder design allows for easy and non-destructive installation of fragile samples, as they are fixed and sealed against bypass flows only by suitable O-rings.

In addition, different inlet and outlet angles are achieved using specially designed and rotatable flow baffles (shown in Figure 2B and lower part of Figure 2C), which force all incoming gases to flow directly along the sample surface and prevent short-circuit flow from inlet to outlet.

In order to further optimize in- and out-flow conditions, the angle between feed/retentate and sweep/permeate flow can additionally be altered by rotating the upper to the lower part of the cell in steps of 30° (from 0 to 180°), so that lower sweep flows can exert a more effective washing effect.

To enable measurements of fluid permeation through a sample, the feed gas can be switched to any external source, such as an evaporator installed inside a mixSorb® (visible on the left side of Figure 2D). In this mode, potential sweep gases are still sup-

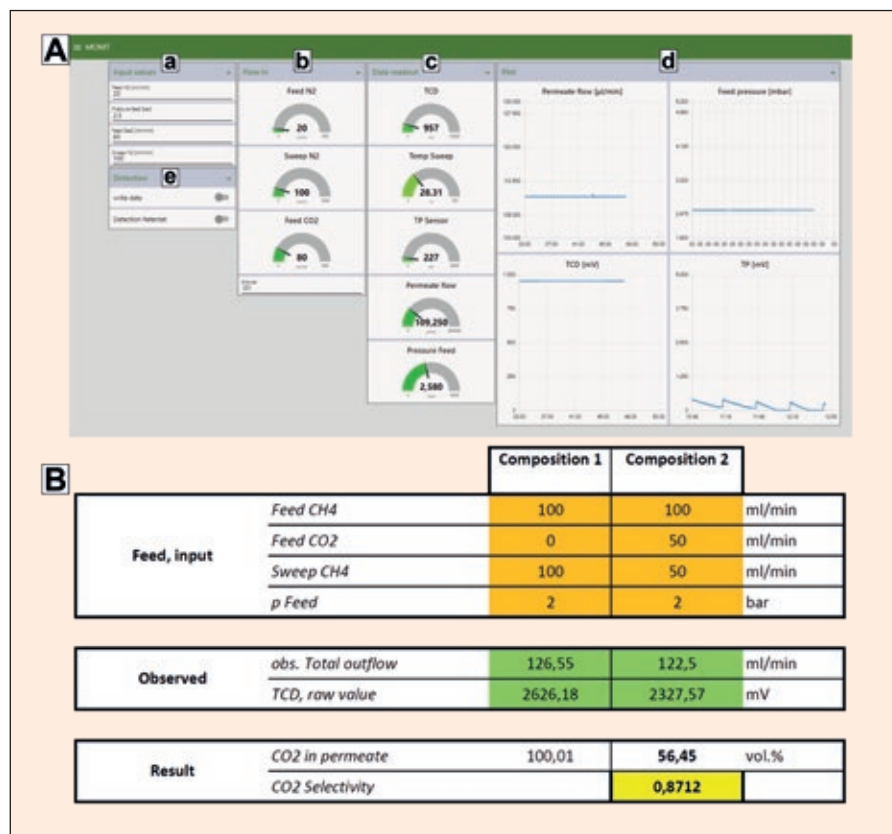


Figure 3 MOMT user interface

A. Interface for the input of setpoints (feed and sweep flows and pressure, see a), graphical visualization of input (b) and data readout (TCD raw value, cell temperature, dew point sensor raw value, outflow value and feed pressure, see c), respective time plots (d) and switches to record data and to switch the detection path

B. Data evaluation interface e.g. for the determination of a membrane's selectivity to gas separation

plied by the instrument. To prevent vapor condensation, a thermostatically controlled tube from the vaporizer to the instrument is recommended. Inside the instrument, the entire area, including the cell and a humidity sensor (a dew point sensor for water vapor measurements), is tempered by an external thermostat and insulated from the environment. The supply gases (feed and sweep) are additionally passed through a heat exchanger connected to the heater and located directly below the cell to ensure its heating.

The instrument is controlled by the electronic modules in the purple area of Figure 2D. Connected to a PC or the local network infrastructure via ethernet, it can be conveniently operated remotely. All adjustments (except those from external devices) are made from the graphical input mask as shown in Fig. 3A-a. Data is recorded to a .csv file upon activation. The acquired data is then manually converted to the desired context using the supplied calibration data (for TCD and dew point sensor) and gas factors.

## Application 1 – Membrane Permeability testing

The permeability of membranes is a relevant feature to predict their general applicability for potential separation processes. Using the presented setup, we have tested different types of porous glass membranes [1] (1 mm thick and 10 mm in diameter) for their permeability to different gases. These are made up by a spongy silicate skeleton with a pore size of around 2 nm and a pore volume of about  $0.15 \text{ cm}^3\text{g}^{-1}$  (referred to as a microporous sample). Further modification by a second thermal alkaline extraction step increases the pore size to about 50 nm and the pore volume to  $0.7 \text{ cm}^3\text{g}^{-1}$  (referred to as mesoporous sample). We have compared both membrane types with respect to their permeability to  $\text{N}_2$ ,  $\text{CO}_2$  and  $\text{CH}_4$  using the instrument under ambient conditions in a dead-end mode.

A pressure resistance test (i.e. observing the increase in feed pressure during continuous feed to the cell and a pressure stability during stopped feed) has to be performed first to verify that the sample is installed correctly, i.e. without any gas bypass, and to test the maximum mechanical stability vs. ambient pressure on the permeate side.

Subsequently the cell should be flushed and the actual permeability experiment can be carried out. For that, both permeate flow and feed pressure is recorded to give a plot as shown in Figure 4A. After converting the permeate flow rate to values in  $\text{mol m}^{-2} \text{ s}^{-1}$  (assuming a permeated cross section diameter of 9 mm), the permeability is obtained from the reciprocal slope obtained from linear regression. Permeability values for the individual membranes in relation to the three gases used are compared in Figure 4B. At this

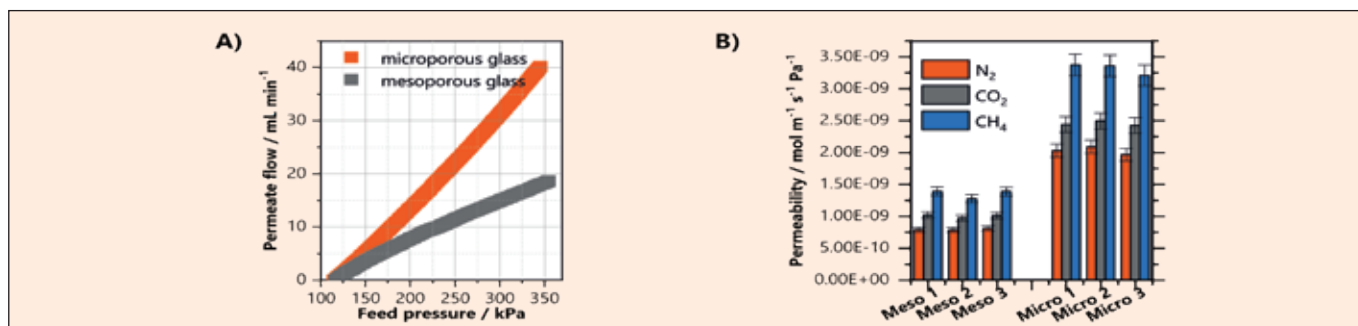


Figure 4 Measurement of permeability of different porous glass membranes

A. Recorded graphs showing the increase of permeate flow with increasing feed pressure upon continuously feeding the cell with  $50 \text{ ml min}^{-1} \text{ N}_2$

B. Permeability values of different membrane types (replicability tests from 3 different batches) and for different pure gases (under consideration of gas factors:  $\text{N}_2$ : 1,  $\text{CO}_2$ : 0.8144  $\text{CH}_4$ : 0.8415)

point it is important to mention that the membranes do not have any separating layer and only the diffusivity is considered. Therefore, the results confirm the expectation that membranes with larger pores and a higher pore volume have a higher permeability than membranes with smaller pores. This is the case for all gases tested, with CH<sub>4</sub> showing the highest permeability through the membranes. This observation can be well explained by the kinetic theory of gases [2]. Figure 4B shows three microporous and three mesoporous membranes. These were all produced according to the same synthesis instructions, but originate from different approaches. Within the error range (5 %), all membranes have the same permeability in relation to the respective gas under investigation. This shows that both the production of the membranes and the measurement itself can be replicated.

## Application 2 – Determination of gas separation potential/ selectivity

Gas separation applications, such as bio-gas upgrading, require highly selective membranes to minimize operating costs through single batch processes. Gas-selective membranes are characterized by large differences in gas permeability between the components to be separated. Therefore, pure gas permeation measurements are a valuable tool to roughly evaluate the applicability of a membrane in such processes. In contrast, the separation of a gas mixture often occurs due to differences in the diffusivity of the components of the mixture. Diffusion-controlled mea-

surements require static and adjustable concentration conditions on both sides of the membrane. For this reason, convincing measurements should take at least diffusional separation effects into account and will also be closer to the final application by using the process-specific gas mixture. Our setup addresses these points, since it can be operated under WK conditions as well as it offers binary (via internal gas supply) up to quaternary gas mixtures (via external gas supply from e.g. a mixSorb® instrument).

As an example, we have tested the separation of a CH<sub>4</sub>-CO<sub>2</sub> mixture using the porous glass membranes described above, i.e. the membrane cell is fed with a defined mixture of both gases. While CO<sub>2</sub> is considered as an impurity, the feed gas composition was varied from 0 vol% to 90 vol% CO<sub>2</sub>. For each composition fed to the cell, the data from TCD and permeate flow were recorded after stable conditions (pressure, TCD value, permeate flow) have been established. The data represent the input for the determination of the apparent CH<sub>4</sub> concentration from the TCD (via calibration). The calculation requires subtracting a sweep gas flow from the total permeate flow, taking a mixed gas factor into account. The resulting permeate gas concentration is then plotted against the given feed gas composition (Figure 5A).

A linear regression within this data gives a slope which is further considered an expression of selectivity, i.e. a slope of 1 means that the membrane allows both gas components to pass through without any difference, i.e. the membrane has no gas selective effect. The other extreme, a

slope of zero, means that only one component (here: CH<sub>4</sub>) can pass the membrane and the other (CO<sub>2</sub>) is blocked. Since, in our case, the selectivity shall express the separation of CO<sub>2</sub> from the mixture, the difference of this slope value from one is further considered as the expression of the selectivity (as in Figure 5B and C).

The measurement results plotted in Figure 5A were obtained under WK conditions, i.e. with an open feed compartment and a sweep gas added to the cell. Figure 5B shows that changing the operating mode results in different selectivity values. This can be taken as an indication of the diffusion influence on the separation effect described above. In addition, it is possible to distinguish between two WK modes: quasi-WK and isobaric-WK (i-WK). The first represents a measurement under WK conditions without a specified feed pressure (i.e. with a pressure adjusted at the pR-R of zero, resulting in a reasonably stable pressure of 1.5 bar due to the cell geometry), while the latter represents a measurement under defined isobaric conditions (i.e. with the respective pressure adjusted, here 2 bar). The results in Figure 5C show that potentially selective membranes can only be identified and characterized with an open feed compartment (as it is the case in both WK modes) and that the pressure set therein should be low to achieve high selectivities. Both results are typically indicative of a diffusion-controlled separation effect. In addition, Figure 5C shows that the selectivity decreases with increasing pressure and lower sweep gas flow. It can be concluded that the pressure effect interferes with the diffusion-driven separa-

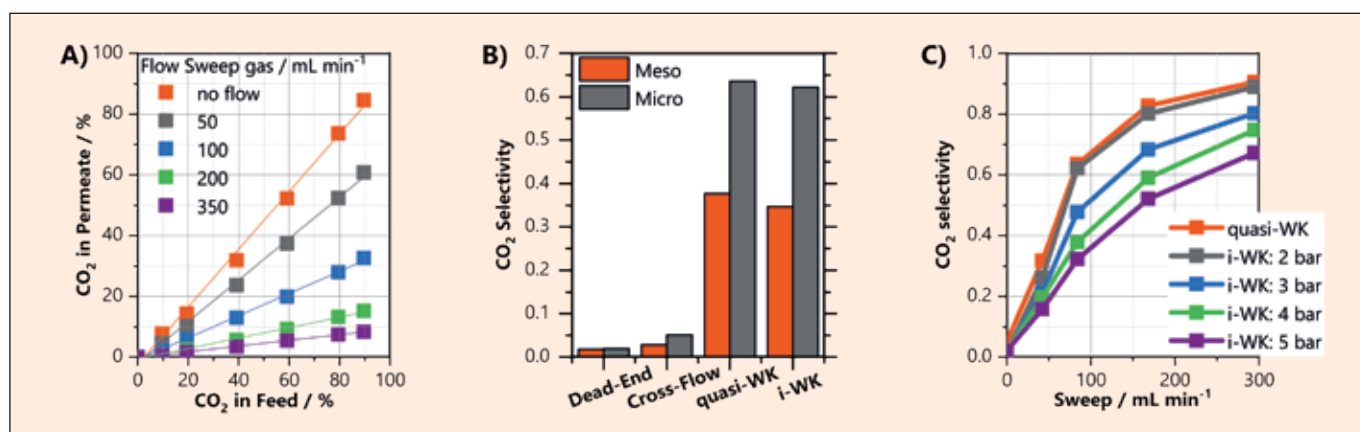


**Figure 5** Separation of CO<sub>2</sub> from CH<sub>4</sub>-CO<sub>2</sub> mixtures using microporous glass membranes  
 A. Example of a composition plot (WK mode) for selectivity determination from the regression slope obtained under varied sweep gas flows (sweep: CH<sub>4</sub>)  
 B. Comparison of different operating modes using the selectivities obtained (for different operating modes in WK mode see text, i-WK mode was obtained under 2 bar feed pressure)  
 C. CO<sub>2</sub> selectivity determined at different sweep flows and feed pressures on a microporous membrane



tion effect, since higher pressures lead to larger permeate flows and thus to lower permeation differences due to different permeabilities and non-selective pressure-driven convection effect. In contrast, the sweep effect verifies the above thesis of a washing effect. The clarity and plausibility of these results show that the MOMT setup provides access to verified gas separation data that can be obtained for different mixtures and membranes.

### Application 3 – Water permeation

A typical application for thin film packaging is the protection of food, cosmetics and other sensitive commodities. While the sealing material is often specific to the content to be protected, moisture protection from the environment is a key concern for many manufacturers.

The characterization of water vapor permeation through various types of films can be achieved with the MOMT setup when a dew point humidity sensor is included in

the tempered region of the instrument (compare with Figure 2D). After calibration, we can determine the permeation of the smallest concentration of water through exchange surfaces of 9 mm diameter. The parameter of interest is the water vapor permeability (WVP), which indicates how many grams of H<sub>2</sub>O can pass through a given area of film per day. To obtain this number, the film sample is installed in the sample holder of the membrane cell, this time with PTFE spacers to ensure gas (and vapor) tightness. The instrument is then connected to an external vapor supply source, in our case a mixSorb® with an evaporator, via a thermostatically controlled connection. All parts, i.e. the evaporator, the manifold of the sorption instrument, the connection and the membrane cell chamber (see Figure 2D, orange area) are tempered to 30 °C and the switch of the feed gas source is turned to external. The temperature is monitored by a sensor in the sweep gas channel. The sweep channel is then purged with N<sub>2</sub> to achieve complete drying of the permeate portion of the instrument.

Water concentration is determined by a dew point sensor capable of determining water concentrations down to 20 ppm. The water vapor concentration is adjusted via the mixSorb Manager® software using N<sub>2</sub> as a "diluent" gas for the saturated vapor produced by the evaporator as well as for the sweep gas. After drying, i.e. when a stable and low plateau of water vapor concentration is observed, the WVP can be obtained by two typical experimental strategies (both in a WK mode with 100 mL min<sup>-1</sup> N<sub>2</sub> sweep flow), hereinafter referred to the pressure step method and the concentration step method.

In strategy 1 (pressure step), the feed at the external source is set to 100 mL min<sup>-1</sup> at 85% rh (relative humidity at 30°C with N<sub>2</sub> as the carrier) and as long as the dew point sensor readings and permeate flow values are unstable no feed pressure is set. The feed pressure is then set at 2 bar until stable sensor readings are measured and then increased in steps to 6 bar (Figure 6A). Water concentrations are continuously recorded and plotted.

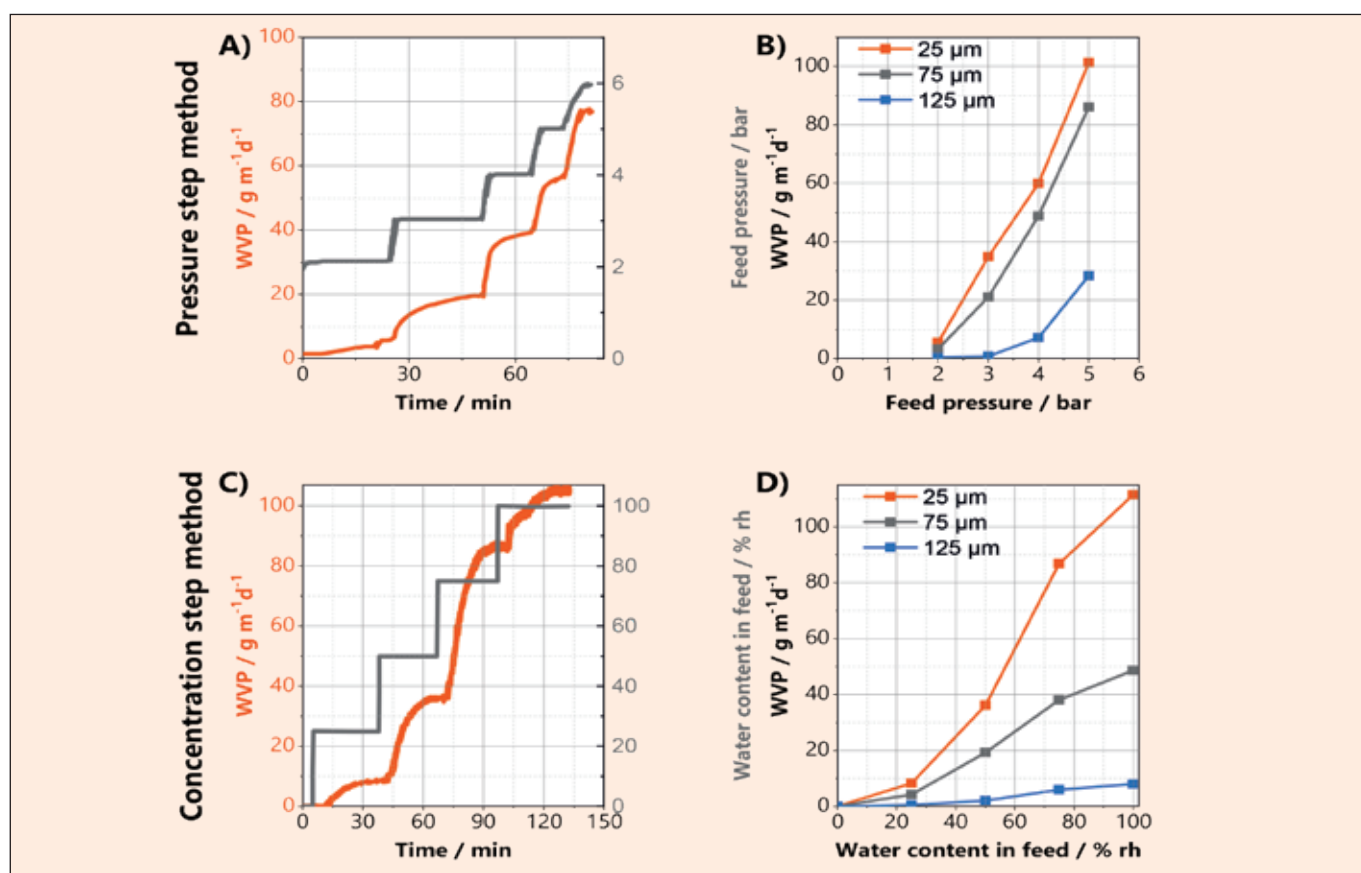


**Figure 6** Results of water vapor permeation through Kapton® foils using the pressure step (A-B) and concentration step method (C-D)  
 A. Real pressure profile (grey) and water vapor permeation (WVP) (orange) as calculated from the dew-point sensor readout (foil thickness: 25 μm)  
 B. WVP vs. applied feed pressure in comparison for different foil thicknesses  
 C. Applied water vapor concentration in feed (grey) and WVP (orange) as calculated from the dew-point sensor readout (foil thickness: 25 μm)  
 D. WVP for different foil thicknesses vs. given Water vapor concentration

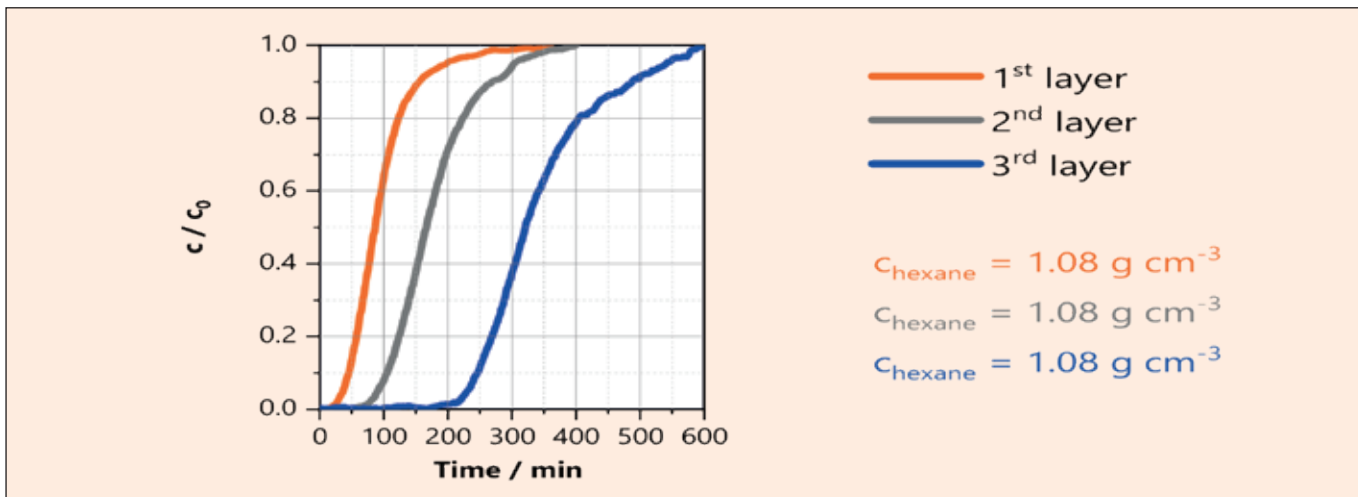


Figure 7 Results of hexane sorption  $c_0 = 1,1 \text{ g m}^{-3}$  on activated carbon fibre material at 25 °C and 70 % rH

In the alternative scenario, the feed initially begins at 0 % relative humidity (rh), with the feed pressure set to e.g. 4 bar. This setting persists until both the dew point sensor and flow meter readings stabilize, ideally reaching a water concentration of 0 ppm after calibration. Subsequently, the feed is gradually adjusted to 25 % rh until stability is achieved, and then progressively increased to 50 %, 75 %, and finally 100 % rh, as illustrated in Figure 6C. In both experiments, the WVP is determined from the dew point sensor reading after calibration and from the flow meter reading after subtracting the sweep gas flow from the total permeate flow. The WVP can be calculated from the water mass flow using the correct exchange area (here a circular area with a diameter of 9 mm). It should be noted that thin foils (we have investigated Kapton® foils of 25 - 125  $\mu\text{m}$  thickness) tend to warp when a static pressure is applied on one side. This warpage (up to 1 mm at 6 bar) increases the exchange area and must be taken into account in the calculation. WVP values corrected in this way are shown in Figure 6. As can be seen, the WVP depends on the applied pressure, water vapor concentration and film thickness. In addition, a possible dependence on the sweep flow could reveal possible diffusion mechanisms. Furthermore, the instrument allows the measurement to be carried out at different cell (and vapor) temperatures, so that kinetic constants of water penetration can be determined and films can be characterized under potentially more realistic conditions.

The consistency of these results (which are comparable to literature values of WVP) and the potential to further extend the measurement to the desired application (regarding film geometry, application temperature, permeant, etc.) clearly demonstrate that the MOMT setup is a versatile alternative to existing and more specified setups.

#### Application 4 – Sorption of Organic Vapors (Dead-end)

As described above for water permeation testing, the MOMT can be installed to the mixSorb used for dosing vapor and/or humidity. Among other applications, this is important for the characterization of respiratory protection filters e.g. based on carbon materials. As an example, by using the dead-end mode with a hexane contaminated carrier gas flow, the breakthrough of hexane vapor at constant temperature and humidity was tested through an activated carbon fibre (ACF), see Fig. 7. Due to the thickness of ACF woven layers it was possible to increase the layer content (one to three layers) and with that, the overall retention time. Sorption capacity can be determined from concentration-time-profiles. Besides the capacities, the MOMT can be used to attribute breakthrough kinetics based on different humidities.

### Summary

We have designed and built a new and highly versatile setup for gas permeation characterization of membranes, called multi-operable membrane test cell (MOMT). It has been shown that the MOMT setup offers great flexibility with respect to

- different permeation application (gas permeation/separation to vapor permeation)
- multiple measurement modes (dead-end, cross-flow, Wicke-Kallenbach and its modifications)
- different scientific permeation questions (determination of permeability, gas separation selectivity, water permeation, or more fundamental aspects such as permeation mechanism and kinetics)
- sample size (thickness: 25  $\mu\text{m}$  - 1 mm, diameter: 10 - 35 mm)
- sample type (micro/mesoporous membranes to non-porous foils), and
- sample material (brittle ceramic membranes to flexible plastic films).

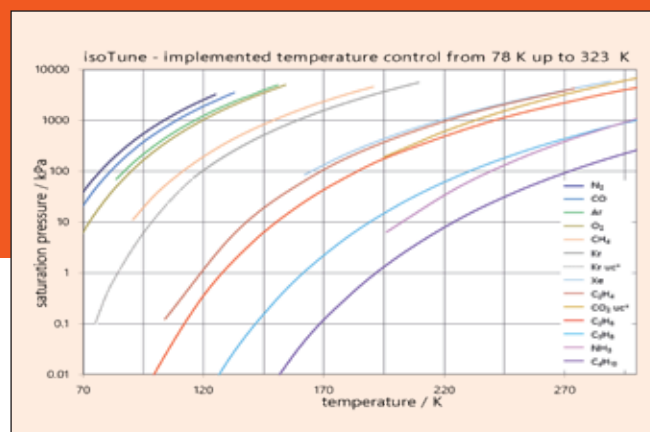
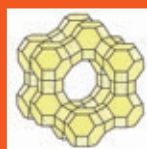
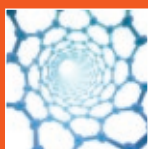
All these features qualify the MOMT cell as the first of its kind and promise both, a broad applicational as well as scientific spectrum.

### References

[1] A. Barascu et al., "Porous glass membranes with an aligned pore system via stretch forming in combination with thermally induced phase separation", *Glass Physics and Chemistry* (2015), 41(1), 73-80.  
 [2] Robert T. Balmer, "Modern Engineering Thermodynamics", Elsevier, 2011.

# The isoTune - The next generation in sorption science

Dr. Carsten Blum, carsten.blum@3P-instruments.com



## Introduction

The isoTune represents a groundbreaking advancement in sorption analysis technology, integrating the outstanding cryoTune principle with the convenience and versatility of a very compact standalone device. In addition, the isoTune can offer a unique fusion of a sorption analyzer and a gas pycnometer to redefine the possibilities of gas and vapor analysis. With unparalleled flexibility, precision, and innovation, the isoTune empowers researchers and industry professionals to explore the depths of sorption phenomena with unprecedented accuracy and efficiency.

### isoTune

#### The Next Generation in Sorption Science

designed to be

- Accurate
- Precise
- Flexible
- Scientific
- Sustainable






**Figure 1** The cryoTune (left) has been the starting point of the isoTunes development and one cryoTune is located in the dewar of the isoTune (right) as the most compact manometric gas and vapor sorption plus density analyzer

## The ideas of the isoTune instrument development

The development of the isoTune has been carried out with the aim to make the analytical instrument more

- **Accurate** (small cold zone for highest sensitivity, no moving dewar with changes of cold zone, cold-warm-transition-zone and of warm zone throughout the full analysis time)
- **Precise** (full thermal control over all components, no moving dewar prevents any temperature change of heat transfer zone over the measuring time and eliminating potential cold-bridges during vapor sorption)
- **Flexible** (easy access to full temperature range for a large set of possible adsorbates and additional capability to carry out accurate density analyses)
- **Scientific** (wide range of possible adsorbates and the potential for seamless, back-to-back measurements with different gases at different temperatures to investigate heats of adsorption among other parameters)
- **Sustainable** (low instrument weight is resource-saving and offers completely new possibilities in after-sales service)

From a theoretical point of view an adsorption process is determined by the difference in chemical potential  $\Delta\mu$  according to

$$\Delta\mu = (\mu_a - \mu_0) = RT \ln \frac{p}{p_0} \quad (1)$$

where  $\mu_a$  is the chemical potential of the adsorbate layer and  $\mu_0$  the chemical potential of the bulk liquid. This difference in potential is related to the ratio of the adsorbates pressure  $p$  and the

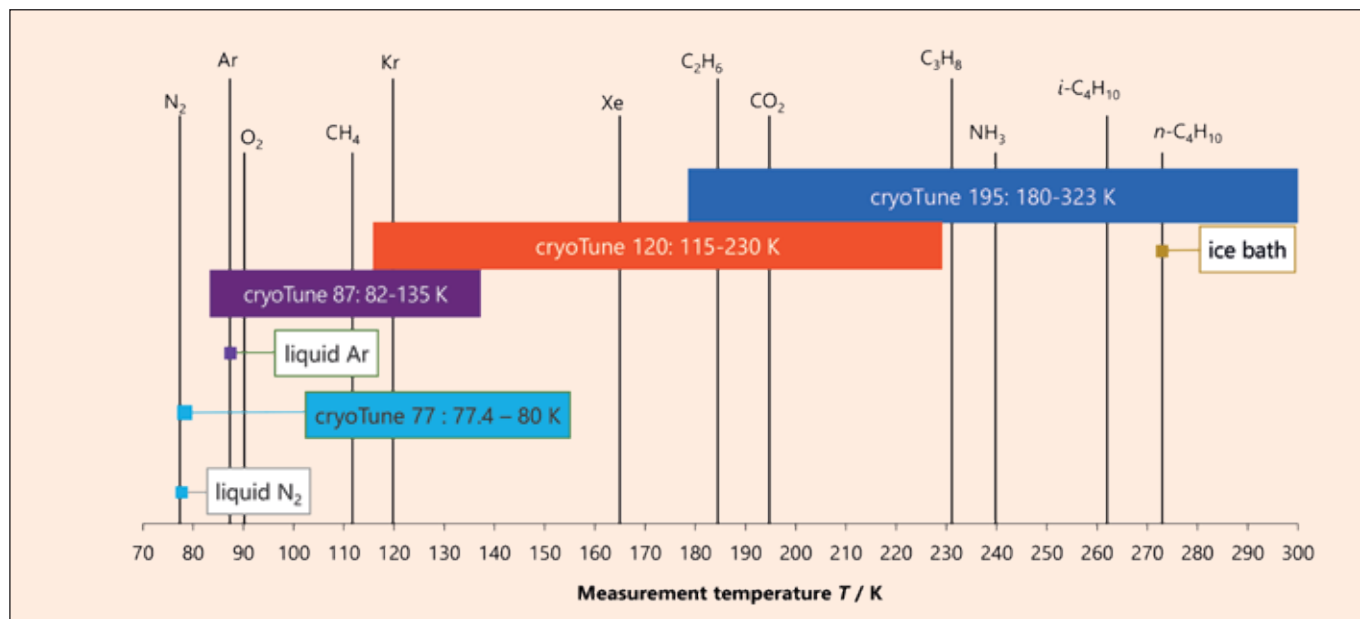


Figure 2 Temperature range of the isoTune

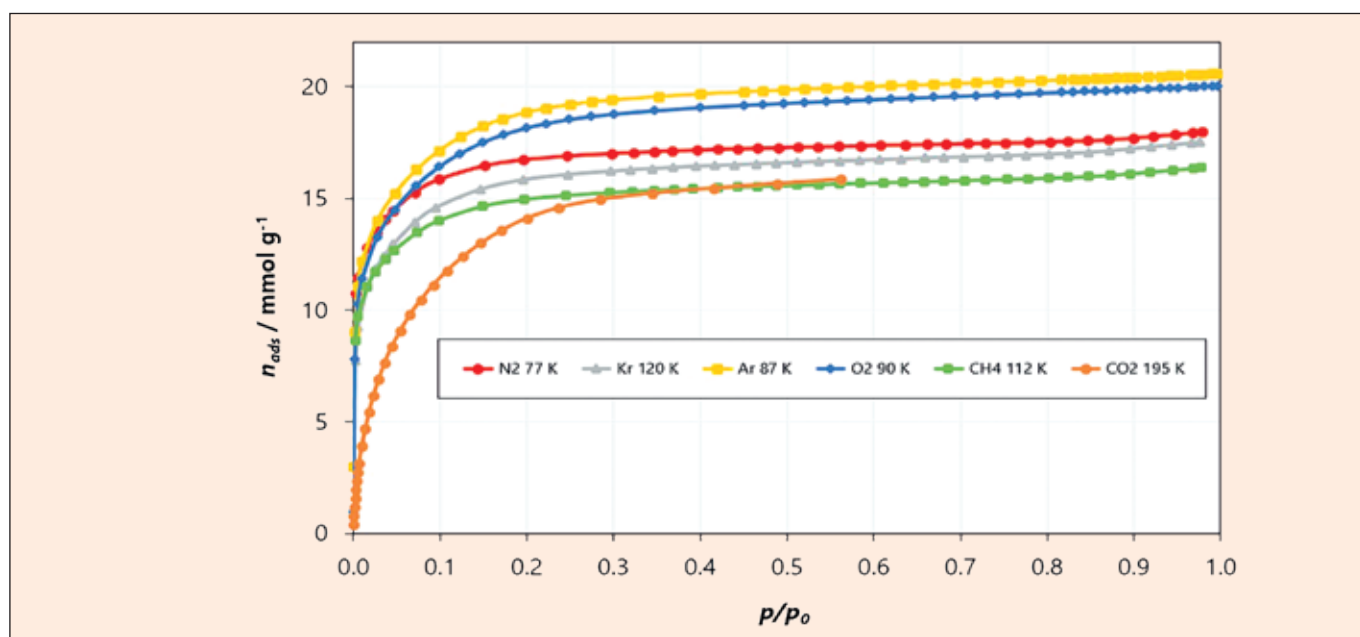


Figure 3 Examples of possible sorption experiments

saturation vapor pressure of the measuring gas  $p_0$  with  $R$  as the universal gas constant and  $T$  the analysis temperature. The adsorbed amount is measured as a function of  $T$ ,  $p$  and  $p_0$  and with the development of a state-of-the-art analyzer of the next generation we have a look at the effects of these parameters on the measurement results, including a detailed consideration of all possible errors. We cannot present all related equations, such as the real gas or thermal transpiration corrections or for the consideration of different temperatures (cold, warm and transition zone) in this article, but we started with the basic parameters in our isoTune development project to hold them as stable as possible. We therefore evaluated both the temperature dependence of the saturation vapor pressures on all possible adsorptives and also the temperature constancy of the measurements. As an

example, specifying the boiling temperature at 77.35 K for liquid nitrogen as the true measuring temperature, as suggested in many technical articles, is actually an unrealistic accuracy if standard cooling with liquid nitrogen is applied directly in contact with the measuring cell. In contrast to that, every user of sorption analyzers can estimate from the determined  $N_2@77K$   $p_0$  values that the measuring temperature is often between 77.0 and 77.6 K and can deviate to higher values as the analysis progresses due to the dissolving of ambient humidity in the cryogenic liquid. All these uncertainties should be avoided as best as possible and perfect stability or the accurate reading of all temperature parameters over the entire measurement period should be recorded and taken into account. Only in this way can error estimates be made on a reliable physical basis and not as black box estimates.

## The isoTune temperature range is based on the cryoTune principle

The cryoTune as the starting point for thermal control of the sample was integrated as a basic component of the isoTune. Inside the cryogenic unit of the isoTune, the measuring cell is not directly immersed in liquid nitrogen, but is instead located in a heat conducting block that can be heated close to the sample and allows heat transfer between measuring cell and liquid nitrogen. Through controlled heating, a temperature range above the boiling point of nitrogen as the measuring temperature can be precisely set and thus different temperatures can be maintained by compensating deviations through adjusting the heater output (see Figure 2). The cryogenic unit of the isoTune provides a substitution of expensive liquefied gases to be used as cryogenic liquids by the consumption of low-cost liquid nitrogen for cooling. This enables the seamless adjustment of any temperature between 77–323 K with a temperature stability better than  $\pm 0.004$  K and long standing times. Sorption studies now extend beyond  $N_2$ , effortlessly measuring Ar,  $O_2$ ,  $CH_4$ , Kr, Xe,  $CO_2$  as well as numerous other gases and vapors with the same simplicity as a standard  $N_2$  isotherm (Figure 3). The isoTunes temperature-dependent adsorptive and adsorbate properties are based on NIST data included in the software, ensuring scientific validity in all measurements conducted.

Some of the most important requirements for maximum accuracy in state-of-the-art manometric sorption analyzers have become the basis of the isoTune instrument development:

- 1. Enabling a flexible temperature control** to use  $N_2@78$ K as traditional basis for comparisons, Ar@87K as recommended method according to [1, 2] and  $CO_2@195$ K or  $CO_2@273$ K for studies of ultramicropores. Temperatures to be varied around 78 K, 87 K and 195 K are used to measure isotherms at different temperatures in order to calculate heats of adsorption while other temperatures are used to measure with krypton, methane or other hydrocarbons at their boiling points for good comparability and to employ the full pressure range and resolution of the instrument.
- 2. No use of so-called filling rods for micropore sorption studies:** The so-called thermal transpiration effect for the lowest pressure range data points can only be scientifically corrected without the use of such fillers [3, 4]. This correction for low pressures requires the free inner diameter of a measuring cell and therefore measurements must be taken in the cold-warm transition zone for correct micropore measurements without fillers.
- 3. No moving temperature control devices** to prevent not only the possible changes of the cold zone, but also strictly prevent changes of the transition area from the cold zone to the warm zone, thus also preventing changes of the warm zone during the measurements. This is especially relevant for long measurements of microporous materials, such as active carbons, MOF's, COF's, pillared clays or zeolites measured without filler rods in the measuring cell as recommended [3, 4] to make use of an accurate thermal transpiration correction.

For measurements to be as accurate as possible, it is essential to keep all cold zone, cold-warm transition zone and the warm zone completely constant during the measurement. Additionally, changes in the ambient temperature that are not taken into account will also contribute to the measurements uncertainty.

- 4. Implementation of a fully temperature-controlled gas pycnometer into the manometric sorption analyzer for accurate density measurements:** The basic method for both gas pycnometry and manometric gas sorption is the same, both are based on employing gas displacement and this pressure relationship is described in the Boyle–Mariotte law. In other words, both methods require one dosing volume and one additional volume containing the sample. The main difference between both methods is, that for density measurements a possible adsorption effect must be prevented, whereas in manometric sorption measurement this effect is supposed to be quantifiable. There are some historical developments to combine both analytical methods in sorption analyzers, but they failed in terms of accurate density results as the instruments volumes were adapted to sorption studies and not to density measurements. This stemmed from the glassware sample cells being in thermal environments not accurately controlled. The fully controlled thermal environment of the isoTunes infrastructure allows for the elimination of such deteriorating effects on gas pycnometry while at the same time reducing the required height for accommodating a dewar lift, thereby also reducing the dead volume exposed to external effects. This allows for the integration of a fully functional gas pycnometer into the system, which in turn benefits from a multi-gas support and highly accurate dosing routines of the sorption analyzer.

## isoTune benefits and advantages over conventional sorption analyzers

### ■ Unique combination of sorption and density measurement analyzer

The isoTune seamlessly integrates a scientific sorption analyzer and gas pycnometer, providing a comprehensive solution for diverse analytical needs. Independently, the general opportunity to measure accurate material densities can enhance sorption studies while allowing ways for special studies with the integrated gas pycnometer such as:

- Use of the standard vacuum connection for the sample preparation in the pycnometer cell
- Use of all connected adsorptive gases for density measurements or to study special effects, e.g. if nitrogen or helium adsorption occurs near room temperature
- Use of the integrated pycnometer allows special kinetic studies of ultraporous materials near room temperature by use of the adsorptives which are available for the sorption device as well.

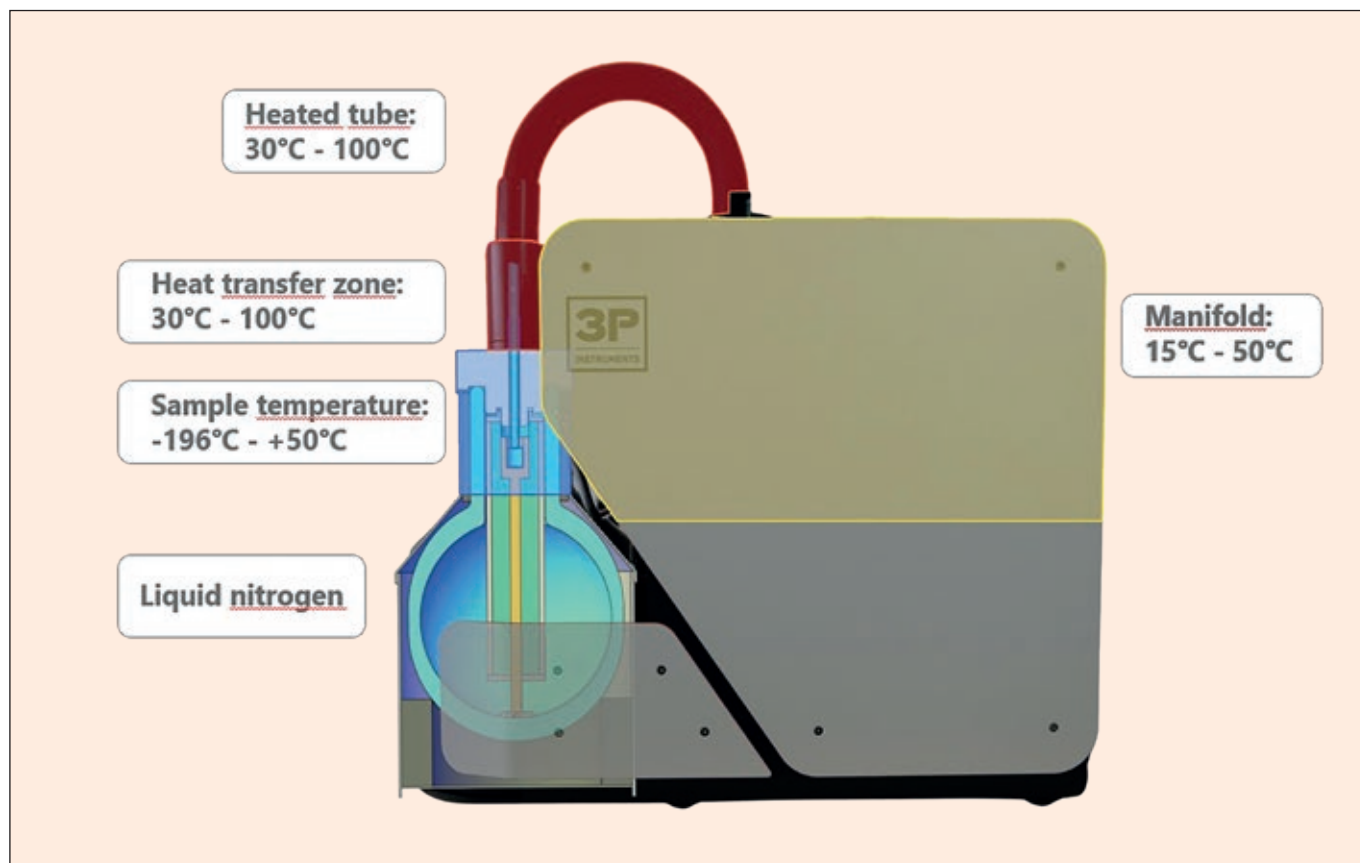


Figure 4 Temperature control over the entire dosing system

■ **Flexible adsorption temperature control**

Sorption of gases and vapors is possible from 77 K up to 323 K, ensuring precise analysis under varying experimental conditions. The isoTune offers unparalleled flexibility to adapt your research requirements with ease.

■ **Integrated gas pycnometer and vapor source**

Enjoy the convenience of an integrated, fully temperature-controlled gas pycnometer for density and specialized sorption measurements. The isoTune's advanced pycnometer utilizes vacuum and all connected gases for sample preparation and specialized analyses, ensuring accuracy and reliability. The measuring cell of the gas pycnometer can be used as a vapor source for vapor sorption measurements, which is an additional feature of a complete isoTune instrument configuration.

■ **Fully controlled thermal environment system**

The isoTune's fully temperature-controlled system eliminates uncertainties from external influences on the environment (Figure 4), a moving dewar or cryogenic liquids' temperature changes, guaranteeing consistent and reliable results with high reproducibility. The cryoTune principle enables a constant small cold zone (-196 °C up to 50 °C, blue) and allows the use of all gases in their respective temperature ranges. The

temperature-controlled transfer zone provides a constant warm zone (30 °C–100 °C) and the heated tube (30 °C–100 °C) eliminates condensation problems (both in red). The temperature in the manifold (upper yellow part with tubes, valves and transducers inside) can be set between 15 °C and 50 °C in order to carry out precise sorption measurements, to prevent vapor condensation in the tubes, and to perform density measurements at well-defined analysis temperatures.

■ **Up to 4 pressure transducers**

For the sorption part of the isoTune, you can choose up to four pressure transducers between the available 0.1, 1, 10, 100, 1000 Torr transducers to find the best combination for your typical application from standard measurements to the determination of smallest surface areas and vapor sorption. The reason for a fourth pressure transducer, especially the 100 Torr transducer, is easy to understand for the case of vapor sorption studies. As example, water at 20 °C has a saturation pressure  $p_0$  of 17.5 Torr and at 45 °C the  $p_0$  value is 72 Torr. Such pressures are to measure more precisely with a 100 Torr transducer instead a 1000 Torr transducer only because the uncertainty of a 1000 Torr transducer to measure between 10 and 100 Torr is about 10 times higher to a 100 Torr transducer.

## Proportional dosing valve

The use of a proportional dosing valve enables precise pressure control of both dose amounts and evacuation rates. The proportional dosing valve method not only speeds up the adsorptive dosing to optimize the measuring time, but also secures the sample handling by preventing elutriation of fine powder particles during evacuation steps.

### ■ Controlled sample transfer

If no sample cell is connected to the measuring port of the analyzer, there is ambient air in the open measuring port and for very critical materials we have to answer the question how to prevent contamination of these residual air (and moisture) components with the sample after connecting the tube to the measuring port. The isoTune features a novel, patent-pending sample transfer mode (Figure 5). Upon triggering sample transfer in the software, the connecting hose is purged with inert gas. Once the sample is attached, the system is automatically evacuated immediately with a user defined evacuation rate. This procedure ensures the exclusion of any sample contamination. Additionally, self-sealing modules are available to further prevent recontamination of activated or sensitive samples.

### ■ Controlled sample preparation

The sample preparation and degassing of the sample prior to the sorption analysis is the basis to measure the sample material as it is and without changes of the pore structure due to this preparation procedure. Linear heating during the sample

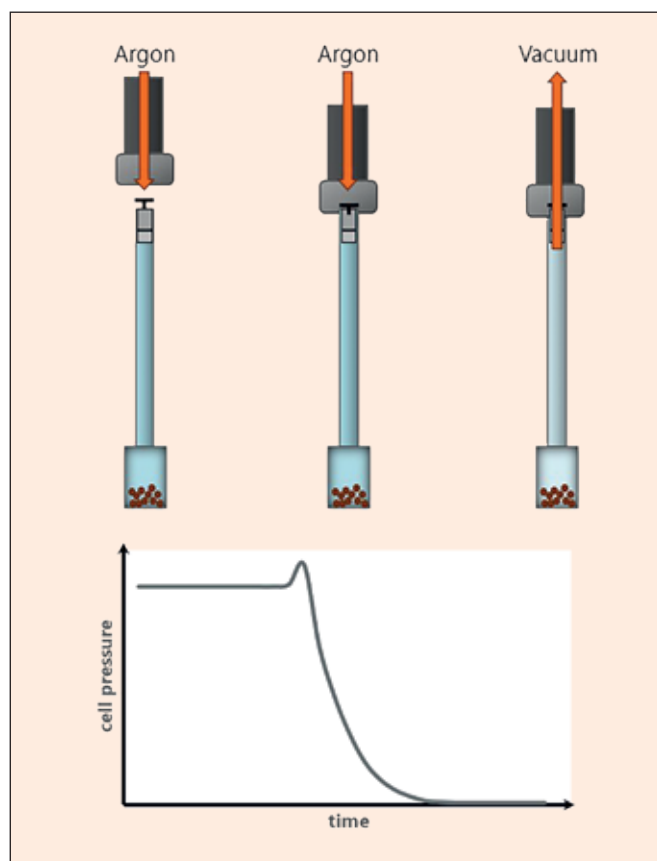


Figure 5 Controlled sample transfer mode

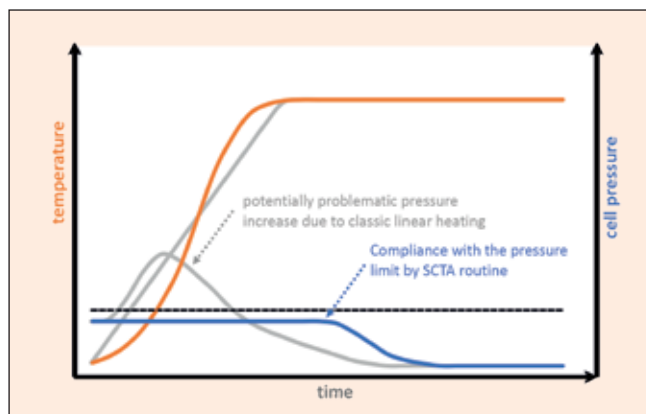


Figure 6 Sample Controlled Thermal Analysis (SCTA)

preparation can cause crystal crack formation due to high pore pressures caused by sudden release of residual moisture and thermal gradients within the sample [6, 7]. A highly reproducible and gentle degassing avoids uncertainty and time-consuming troubleshooting in case of poor measurement reproducibility of special materials. Utilizing the Sample Controlled Thermal Analysis (SCTA) routine described by J. Rouquerol et al [5], the isoTune ensures that sample preparation is precisely controlled by the sample itself. Figure 6 illustrates the difference to classical constant heating rates and corresponding cell pressure in the sample cell (grey, with overshooting pressure range). The heating rate (orange) is controlled by the evaporation or desorption rate of the sample (blue) by defining a fixed pressure limit (dotted line, the blue pressure curve never shoots beyond that line).

## Summary

During the development of the new manometric sorption isoTune analyzer, all steps of the manometric measurement process, including sample preparation, were thought out using state-of-the-art technology and updated according to best scientific practices. With the approach of the isoTune 3P Instruments has developed the next generation state-of-the-art manometric sorption analyzer. With the isoTune there are opportunities for all research labs available to use the almost perfect measurement technology directly, or within the scope of contract measurements in our LabSPA (Lab for Scientific Particle Analysis). Feel free to contact [info@3P-Instruments.com](mailto:info@3P-Instruments.com) for further information.

## References

- [1] ISO 9277:2010: Determination of the specific surface area of solids by gas adsorption – BET method
- [2] IUPAC Technical report, Pure Appl. Chem. 87(9-10), 1051-1069 (2015) Thermodynamics", Elsevier, 2011.
- [3] P.A. Webb, C. Orr, Analytical Methods in Fine Particle Technology, Micromeritics Instrument Corp., Norcross, GA, USA, p. 107
- [4] S. Lowell et al, Characterization of porous solids and powders, Kluwer 2004, p. 254
- [5] J. Rouquerol, "Thermal Analysis: Sample-Controlled Techniques" in: Encyclopedia of Analytical Science (3rd Ed.)
- [6] F. Rouquerol, J. Rouquerol, K. S. W. Sing, P. Llewellyn, G. Maurin, Adsorption by powders and porous solids: principles, methodology and applications, 2nd edition, Academic Press, 2014, p. 626
- [7] T.O. Sorensen, J. Rouquerol, Sample Controlled Thermal Analysis (SCTA): principle, origins, goals, multiple forms, applications and future, Kluwer Academic Publishers, Dordrecht, 2003, p. 252

Zeta Potential

Tapped Density

BenchCat Reactor Systems

Powder Characterization

Vapor Sorption Breakthrough Curves

Stability Index of Dispersions

BET Surface Area

Density

Gas Pycnometry

Contract Analysis

Micro rheology

Molecular Weight

Dynamic Image Analysis

Chemisorption

Temperature

Programmed Techniques

Laser Diffraction

Pore Analysis

Particle Shape



Characterization of particles • powders • pores

Particle Size Gas Sorption

Nanoparticle Analysis

Dynamic Light Scattering

Conductivity

Electroacoustics

Electrophoretic Light Scattering

Water Vapor Sorption



3P Instruments GmbH & Co. KG

Rudolf-Diesel-Straße 12  
85235 Odelzhausen | Germany  
Tel. +49 8134 9324 0  
info@3P-instruments.com

www.3P-instruments.com

@3P\_Instruments

3P-Instruments

ISSN 2750-7084 (Print)  
ISSN 2750-7092 (Online)